REVIEW ARTICLE

Plasma deposition of optical films and coatings: A review

Ludvik Martinu[a)]
Groupe de Recherche en Physique et Technologie des Couches Minces (GCM) and Department of Engineering Physics and Materials Engineering, École Polytechnique, C.P. 6079, Station Centre-Ville, Montréal, Québec H3C 3A7, Canada

Daniel Poitras
Institute for Microstructural Sciences, National Research Council of Canada, Ottawa, Ontario K1A 0R6, Canada

(Received 4 August 2000; accepted 7 August 2000)

Plasma enhanced chemical vapor deposition (PECVD) is being increasingly used for the fabrication of transparent dielectric optical films and coatings. This involves single-layer, multilayer, graded index, and nanocomposite optical thin film systems for applications such as optical filters, antireflective coatings, optical waveguides, and others. Beside their basic optical properties (refractive index, extinction coefficient, optical loss), these systems very frequently offer other desirable ''functional'' characteristics. These include hardness, scratch, abrasion, and erosion resistance, improved adhesion to various technologically important substrate materials such as polymers, hydrophobicity or hydrophilicity, long-term chemical, thermal, and environmental stability, gas and vapor impermeability, and others. In the present article, we critically review the advances in the development of plasma processes and plasma systems for the synthesis of thin film high and low index optical materials, and in the control of plasma–surface interactions leading to desired film microstructures. We particularly underline those specificities of PECVD, which distinguish it from other conventional techniques for producing optical films (mainly physical vapor deposition), such as fabrication of graded index (inhomogeneous) layers, control of interfaces, high deposition rate at low temperature, enhanced mechanical and other functional characteristics, and industrial scaleup. Advances in this field are illustrated by selected examples of PECVD of antireflective coatings, rugate filters, integrated optical devices, and others. © *2000 American Vacuum Society.* [S0734-2101(00)03606-X]

I. INTRODUCTION

The development of the physics and technology of thin films has significantly been stimulated by their use in optical systems for numerous conventional and high-tech applications. This includes, in particular, transparent dielectric coatings for optical filters [in a broad sense: devices selecting a portion of the transmitted or reflected light, such as antireflective (AR) coatings, band pass filters, edge filters, hot/cold mirrors and others][1–4] and optical waveguides.[5,6] For example, close to 70% of glass production worldwide, flat glass (e.g., window glass, picture glass, laminated glass, motor vehicle windshields and windows, skylight glass, etc.) and shaped glass (for example, lenses for precision instruments and for ophthalmic applications), are provided with AR coatings, optical filters for thermal control, or decorative coatings. The flat glass production worldwide is about 10^9 m^2/yr (almost half of it in the USA), which represents a U.S. market value of several billions of US dollars.[7,8] In addition, the rapidly evolving area of advanced applications includes very narrow band filters (<1 nm) for wavelength division multiplexing,[9] interference color-shifting films[10,11] and pigments[12] for antiforgery devices, low laser damage filters, chirped mirrors for ultrashort laser pulse compression,[13,14] integrated optics for optical signal processing in optical communication, optical computing and optical sensors, and others.

In order to qualify for optical applications, the following criteria should be respected when choosing the appropriate film material and film deposition process:

(i) The technique must allow good control and reproducibility of the complex refractive index

$$N(\lambda)=n(\lambda)-ik(\lambda). \quad (1)$$

The wavelength dependence of the refractive index $n(\lambda)$ and the extinction coefficient $k(\lambda)$ is governed by the dispersion relations, which depend on the material's microstructure. In practical applications the n values should be precisely controlled to the second decimal for filters, and to the third decimal for waveguides. In transparent filters, required $k(\lambda)$ values are usually around or below 10^{-4}, and the optical loss in waveguides should generally be well below 1 dB/cm. In all optical film applications, at least two basic materials must be available which possess high (n_H) and low (n_L) indices; they are frequently complemented by a third, medium (n_M) index material. A large (n_H-n_L) value may help reduce the design thickness and improve the performance of filters.

[a)]Author to whom correspondence should be addressed; electronic mail: lmartinu@mail.polymtl.ca

(ii) In most optical coatings applications, materials are desired to be amorphous, isotropic, and with no birefringence, for keeping scattering below 10^{-4}.

(iii) The optical film must fulfill certain minimum mechanical requirements; these include (a) good adhesion (evaluated using an adhesive tape peel test, frequently applied after sample exposure to a humid environment at elevated temperature), (b) acceptable scratch and abrasion resistance to allow handling (for example, by performing a cheese cloth rubbing test), (c) acceptable stress (typically 0–500 MPa in compression), and (d) absence of cracks.

(iv) The fabrication methods are frequently required to achieve good film thickness uniformity across the coated part (below 3%, or below 1% for high-precision applications, e.g., filters for telecommunications), an acceptable deposition rate (~1 nm/s), and good environmental stability.

Optical filters have traditionally been fabricated by physical vapor deposition (PVD) techniques such as evaporation and sputtering, frequently assisted by ion bombardment [ion plating, ion beam assisted deposition, unbalanced magnetron sputtering, (filtered) cathodic arc deposition etc.], as described in numerous earlier reviews.[15,16] Sol–gel deposition is also considered to be an alternative route. Beside PVD and sol–gel, other techniques have been employed for the fabrication of film materials for optical waveguides; they are flame hydrolysis, ion implantation, ion exchange, mixing, doping, implantation, and others (for reviews, see for example Refs. 5, 6 and 17).

Plasma enhanced chemical vapor deposition (PECVD)—i.e., film growth using gas phase precursors activated in a glow discharge environment—has been employed industrially in microelectronics for several decades. Its industrial acceptance in other areas such as optical films and coatings has been delayed mainly due to the complexity of the plasma–chemical reactions and plasma–surface interactions, due to insufficient process control, and to relatively high equipment cost. However, recent advances in low pressure plasma processing, and in PECVD in particular, have greatly increased the interest in PECVD for the fabrication of optical films, and its industrial use has been successfully demonstrated.[18–20] Not only can PECVD provide materials with optical characteristics similar to those obtained by their PVD counterparts, but the PECVD processes can address numerous novel aspects of optical film deposition. The main driving force and stimulation for such interest resides with the following attributes:

(i) Widely ranging control of plasma–chemical reactions and plasma–surface interactions allow one to optimize the film composition and microstructure: the films generally possess high packing density (>98%), and are therefore hard and environmentally stable. This can be achieved by tailoring the energetic interaction between the plasma and the surface, by using bias-controlled or pulsed plasma techniques. In one deposition reactor one can fabricate a multifunctional system (schematically illustrated in Fig. 1) providing the desired optical effect (e.g., filter, AR coating, or optical waveguide), complemented, for example, by enhanced scratch resistance, gas or vapor impermeability, and surface hydrophobicity (or hydrophilicity).

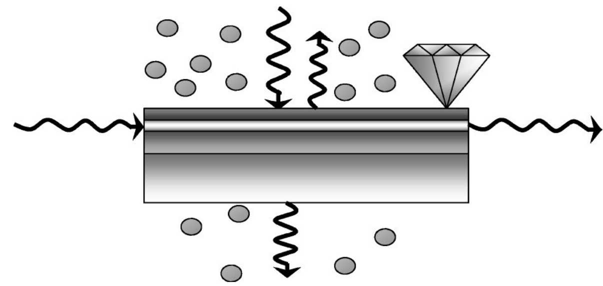

FIG. 1. Schematic illustration of multifunctional character of a multilayer thin film system.

(ii) PECVD is suitable for the fabrication of films with a desired intermediate n value and of inhomogeneous (graded index) optical films, in which the refractive index n continuously varies as a function of depth z. The most significant optical filters of this kind use rugate[21] filter designs, where $n(z)$ varies continuously between high and low n values.[22,23] The absence of abrupt index changes (or abrupt interfaces) leads to the suppression of harmonics, and an appropriate apodization (envelope) function helps suppress side lobes outside the band-pass wavelength (see Sec. V). In addition, the absence of sharp interfaces leads to a uniform distribution (or compensation) of internal stresses, generally leading to enhanced adhesion and mechanical integrity.

(iii) PECVD provides high deposition rates (1–10 nm/s, or more), substantially higher than other, more traditional techniques (e.g., PVD), in particular for high index materials. This aspect is the basis for a reliable low-cost fabrication technology.

(iv) Different substrate shapes can be uniformly coated (flat, hemispherical, cylindrical shapes, the interior of tubes, etc.).

(v) PECVD films generally possess better mechanical properties than their PVD counterparts. This applies in particular to films deposited on plastic substrates, where the existence of a physically thick, graded interfacial region containing covalent bonds leads to substantially enhanced film adhesion, stress compensation, and scratch, abrasion, and wear resistance.[24] Surface modification of polymers using low pressure plasma processes for improving adhesion is an expanding area in itself.[25,26]

(vi) The PECVD process allows doping to control optical selectivity, electrical conductivity, or optical nonlinearity. This can be accomplished by introducing additives to the gas phase, or by a combination with other deposition techniques in a hybrid reactor, whereby a ''dopant'' is incorporated via simultaneous cosputtering, coevaporation, or other approaches.[27]

(vii) The use of PECVD is attractive for the fabrication of optical waveguides and integrated optical devices.[17] PECVD is already fully compatible with the existing silicon-based semiconductor technology (patterning, etching), so that both optical and electronic devices can be combined on one chip; waveguides are suitable for pigtailing (low insertion loss

leading to efficient fiber-to-chip coupling), and the deposition process occurs at low temperatures (<300 °C, substantially below the sol–gel process, >500 °C, for example).

The objective of the present article is to critically review the advances in PECVD of transparent dielectric films and coatings for optical applications such as optical filters and optical waveguides, which can be implemented in devices operating in a wavelength range from near ultraviolet (~300 nm) to near infrared [(NIR)~1700 nm] regions. Clearly, the frontiers between optical coatings and other fields of optics and physics are difficult to define; because of space limitations and in order to maintain the focus, only brief mention will be made of semiconductors and optically active materials fabricated by PECVD. It is not the intention of the authors to give a complete bibliography of the optical properties of plasma-deposited films, but rather to point out the main trends and open questions in this field, frequently illustrated by results from publications that clearly demonstrate the suitability of processes and materials for optical use [for example, the $n(\lambda)$ and $k(\lambda)$ dispersion curves]. We begin with a categorization of plasma-deposited optical materials and a description of basic plasma processes and plasma systems (Sec. II). This is followed by a detailed overview of the optical (Sec. III) and mechanical (Sec. IV) characteristics of plasma-deposited optical films. Particular attention is paid to the films' structure–property relationships, their functional characteristics, and their performance on plastic substrates, the latter being related to the existence of an interphase. Applications are illustrated by examples of optical devices (Sec. V), followed by a summary of the prospects for (*in situ*) process control and industrial scaleup (Sec. VI).

II. PLASMA PROCESSES AND PLASMA SYSTEMS

Optical and other characteristics of plasma-deposited materials depend on the choice of the precursor gases or vapors, and on plasma–surface interactions during film fabrication. The former aspect mainly defines the film composition, while the latter is closely related to the film growth energetics and, consequently, the resulting packing density, stress, stability, etc. The vast majority of PECVD materials are amorphous, since they are deposited at low substrate temperature, typically below 250 °C.

The refractive index values of the most frequently studied PECVD materials are summarized in Fig. 2; clearly, they cover the whole range required for successful interference filter application. For comparison, the most often used transparent PVD and substrate materials are also shown. Beside the traditional glass, substrate materials also include polycarbonate (PC), poly(methyl methacrylate) (PMMA), and poly(ethylene terephthalate) (PET), which are increasingly employed in the optics industry (for example, ophthalmic lenses, windshields, optical transducers, etc.) because of their beneficial optical (low absorption, $k<10^{-3}$ at 550 nm) and bulk mechanical characteristics (e.g., low weight, high impact resistance).[28]

PECVD materials can be either inorganic or organic in nature, depending on the precursor gas or vapor, and on the

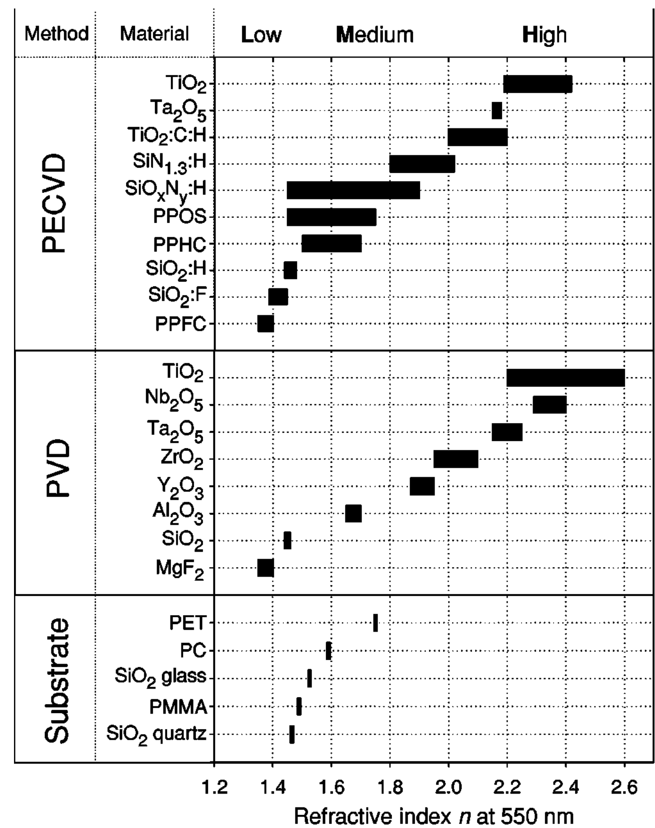

FIG. 2. Refractive index (at λ=550 nm) of different PECVD optical film materials; comparison with selected substrate and PVD materials.

fabrication conditions. The most thoroughly studied precursors which have been explored as candidates for optical materials are summarized in Table I. Many films tend to contain a certain concentration of hydrogen, for example, the amorphous hydrogenated silicon dioxide (SiO_2:H), nitride ($SiN_{1.3}$:H), and oxynitride (SiO_xN_y:H). Some of the materials retain some ''organic'' character by containing residual carbon from organosilicone or other precursors, for example SiO_2:C:H. A particular category of low-index films from organic precursors are the so-called plasma-polymerized hydrocarbons (PPHCs), plasma-polymerized organosilicones (PPOSs), and plasma-polymerized fluorocarbons (PPFCs). On the high index side, the most important examples are titanium dioxide and tantalum pentoxide, derived from halides (TiO_2, Ta_2O_5) or from organometallic precursors (TiO_2:C:H;Ta_2O_5:C:H). For completeness, we also show hard hydrogenated amorphous carbon (a-C:H) films frequently referred to as diamond-like carbon (DLC). However, this latter material is absorbing in the visible region (see Sec. III); it cannot readily be applied in usual filter designs in the visible region, but it is often used for applications in the NIR, due to its excellent mechanical characteristics (e.g., high hardness and low friction, see Sec. IV), which are very beneficial for numerous applications (for example, as optical windows for laser barcode readers in supermarkets).

Before we proceed further with describing the optical performance of the above-mentioned materials and its relation to their microstructure, it is important to discuss plasma sys-

TABLE I. Precursors and refractive index values for selected reported transparent plasma-deposited optical materials.

Material	Precursors	Remark	n(550 nm)
SiO_2:H	silane/oxygen or nitrous oxide SiH_4/O_2 or N_2O	gas (hazardous, flammable)	1.456–1.480
SiO_2:H:C	tetraethoxysilane (TEOS): $Si(OC_2H_5)_4$	liquid	
	hexamethyldisiloxane (HMDSO)	liquid	1.47–1.50
	tetramethyldisiloxane (TMDSO)	liquid	
SiO_2:F	$SiH_4/O_2/CF_4$	gas	
SiO_2:F:C	TEOS/C_2F_6	liquid/gas	1.41–1.47
	TEOS/O_2/CF_4	liquid/gas	
	fluorotriethoxysilane (FTES): $(C_2H_5O)_3SiF$	liquid	
PPFC	C_2F_4, C_4F_8, etc.	gas	1.35–1.38
	hexafluoropropylene (HEPO)	liquid	
	fluoro-alkyl silanes (FASs)	liquid	
	perfluoro-1,3-dimethylcyclohexane (PFDCH)	liquid	
Al_2O_3	aluminum chloride: $AlCl_3/O_2$ or N_2O	solid (corrosive)	1.54–1.62
Al_2O_3:C:H	trimethyl-aluminum (TMA): $(CH_3)_3Al/O_2$ or N_2O	liquid	1.54–1.64
	trimethyl-amine alane (TMAA): $(CH_3)_3NAlH_3/O_2$ or N_2O	liquid (react with water)	
$SiN_{1.3}$:H	SiH_4/N_2 (or NH_3)	gas	1.79–2.04
$SiN_{1.3}$:H:C	hexamethyldisilazane (HMDSN)	liquid	1.75
	hexamethylcyclotrisilazane (HMCTSZN): $[SiN_{1.3}H(CH_3)_2]_3$	liquid	
SiO_xN_y:H	$SiH_4/O_2/N_2$ or $SiH_4/N_2O/NH_3$	gas	1.46–2.05
AlO_xN_y	$AlBr_3/H_2/N_2O$	gas	1.60–2.10
TiO_2	titanium tetrachloride: $TiCl_4/O_2$	liquid (corrosive)	2.20–2.45
TiO_2:C:H	tetraisopropyltitanate (TIPT): $Ti(OC_3H_7)_4/O_2$	liquid	
	tetraethoxytitanate (TEOT): $Ti(C_2H_5)_4/O_2$	liquid	
Ta_2O_5	TaF_5/O_2	solid	2.12–2.16
Ta_2O_5:H:C	tantalum pentaethoxide: $Ta(OC_2H_5)_5/O_2$	liquid	
	$Ta(OCH_3)_5/O_2$	liquid	
a-C:H	methane CH_4, C_nH_{2n+2}, C_nH_{2n}, etc.	gas, liquid	1.6–2.20
GeO_2:H:C	tetramethylgermanium (TMGe): $Ge(CH_3)_4/O_2$	liquid	1.463–1.477
Y_2O_3-ZrO_2 (YSZ)	acetylacetonatozirconium Zr(acac)$_4$: $(C_5H_7O_2)_4Zr$	solid melts at 467 K	2.10
	dipivaloylmethanato yttrium Y(dpm)$_3$: $(C_{11}H_{19}O_2)_3Y$	solid melts at 442 K	
$BaTiO_3$	dipivaloylmethanate barium Ba(dpm)$_2$: $(C_{11}H_{19}O_2)_3Y$/TIPT/O_2	solid melts at 455 K	2.19
$SrTiO_3$	dipivaloylmethanate strontium Sr(dpm)$_2$: $(C_{11}H_{19}O_2)_3Y$/TIPT/O_2	solid melts at 410 K	2.19

tems and basic processes for film fabrication.

In spite of the proliferation of low-pressure plasma processes already in use, or having potential for near or longer term industrial application, there are still important, yet unresolved questions regarding the most efficient use of plasma. Reasons for this are the relative novelty of plasma, on the one hand, and its inherent complexity on the other. To ensure high quality and reproducibility of a given plasma

process, numerous parameters must be controlled;[29] these include so-called ''external'' parameters like pressure, gas flow, excitation frequency, power, and the resulting ''internal'' (bulk) plasma characteristics, namely the electron density, n_e, and the electron energy distribution function (EEDF). During deposition, the bulk plasma parameters generally control the rate at which chemically active precursor species (molecular fragments—free radicals) and energetic species (electrons, ions, photons) are created. In combination with the type of selected gases, gas-phase chemical processes are largely responsible for the chemical composition of the films deposited, along with plasma–surface interactions and substrate surface conditions, which dictate film microstructure.

An important factor influencing the processing plasma is the discharge field frequency $f=\omega/2\pi$. Most frequently, high frequency plasmas ($f>1$ MHz) are used for PECVD of dielectric optical films, in order to avoid surface charging and plasma instabilities, namely ITU (International Telecommunications Union)-approved industrial, scientific, and medical frequencies [13.56 MHz radiofrequency (rf), or 2.45 GHz microwave (MW)].[30] Interestingly, high-quality optical film materials have mostly been obtained in MW rather than rf plasmas, using different reactor designs illustrated in Fig. 3.

MW and rf discharges differ mostly in their EEDFs, which can be obtained by solving the Boltzmann equation; these have shown that the population of electrons in the high-energy tail of the EEDF is higher in MW plasma than in its rf counterpart.[31] The number of electron–ion pairs formed per unit of delivered energy is highest when the EEDF is Maxwellian, a condition fairly well obeyed in MW plasma. In addition, the MW plasma is controlled by ambipolar diffusion, i.e., the electron–electron collisions prevail, while in rf plasma, a mobility-controlled discharge, the energy loss is due to direct charged particle impact on the walls. As a consequence, the ionization and dissociation rates are higher in the MW discharge, generally leading to a higher deposition rate and a higher ion flux (see below).

We have pointed out above that the reactor type, namely MW versus rf plasma, influences the fundamental plasma properties such as the EEDF; however, it also has an important effect on how the plasma interacts with the exposed surface. Surfaces in contact with a plasma exhibit an interfacing medium, the plasma sheath, which is electrically nonneutral in contrast to plasma itself. The surface is at a floating potential V_f, with respect to plasma potential V_p. Since $V_f<V_p$, positive ions are accelerated from the plasma to the surface, while some of the electrons are repelled. However, under steady-state conditions, there is no net current flowing, since ion and electron fluxes are then equal. In this case, the thickness of the sheath is a few times the Debye length, and it grows with increasing average electron energy and decreasing electron density.

Assuming, for simplicity, the EEDF to be Maxwellian and the surface immersed in the plasma to be a plane, the potential difference across the sheath can then be approximated by[32]

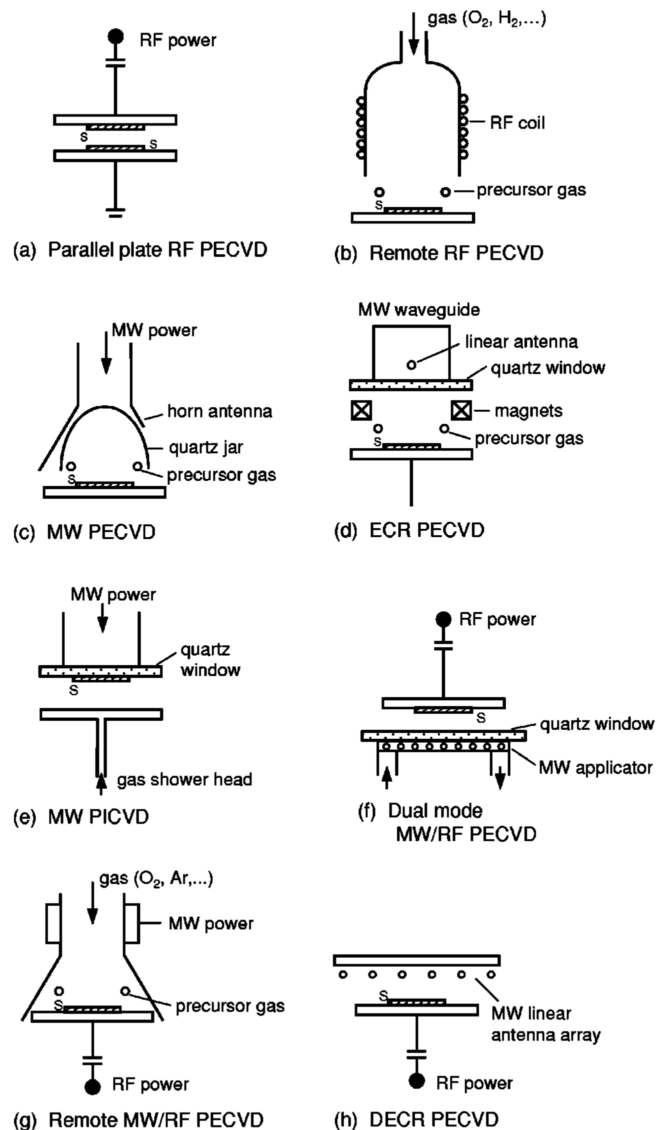

FIG. 3. Schematic illustration of different types of high frequency plasma systems for PECVD of optical films: (a) asymmetric capacitively coupled rf plasma; (b) remote plasma rf reactor; (c) MW plasma reactor with different excitation components (antenna, standing wave applicator, traveling wave applicator) used in a cw or pulsed modes; (d) ECR plasma reactor; (e) MW PICVD reactor for planar substrates; (f) dual-mode (pulsed) microwave/radiofrequency (MW/rf) plasma system; (g) remote MW/rf plasma system; (h) DECR PECVD system.

$$V_p-V_f=\frac{k_BT_e}{2e}\ln\left(\frac{m_i}{2\pi m_e}\right), \tag{2}$$

where k_B is the Boltzmann constant, T_e is the electron temperature, e is the electron charge, and m_i and m_e are the mass of ions and electrons, respectively. We note that on floating potential surfaces, the ion energy $E_i=e(V_p-V_f)$ is typically a few times the electron temperature expressed in electron volts. It also shows that the ions always acquire some additional energy as they pass through the sheath on their way to the surface.

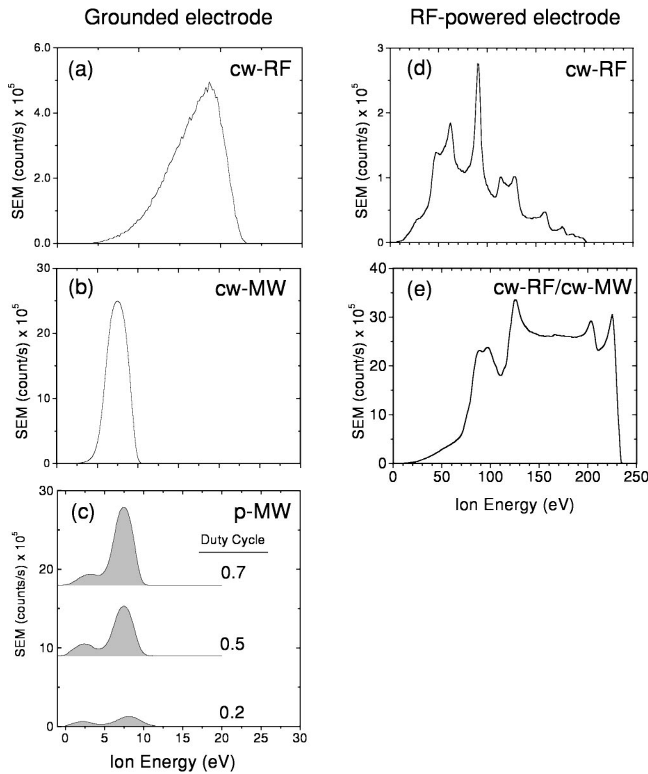

FIG. 4. Examples of the IEDFs of Ar^+ ions in high frequency plasma in argon at 60 mTorr measured in the following configurations: (a) grounded electrode in cw-rf discharge such as in the reactor from Fig. 3(a) ($V_B = -150$ V); (b) grounded electrode in cw-MW discharge such as in the reactor from Fig. 3(f) ($P_{MW} = 300$ W); (c) grounded electrode in a pulsed MW discharge in the reactor from Fig. 3(f) using different duty cycles ($P_{MW} = 300$ W); (d) rf-powered electrode in a cw-rf discharge such as in the reactor from Fig. 3(a) ($V_B = -150$ V); and (e) rf-powered electrode in a dual-mode cw-rf/cw-MW discharge in the reactor from Fig. 3(f) ($V_B = -150$ V, $P_{MW} = 300$ W). (Modified after Ref. 45.)

The energy of the charged particles impinging on a substrate can be adjusted by biasing it at a potential V_B with respect to V_p. For the case of an insulating material (of the main interest in the present context), it can only be biased by applying a periodic voltage. The substrate surface exposed to the plasma is then capacitively charged, that is, electrically polarized, providing a mean dc voltage component V_B. If the frequency of the applied periodic voltage f is greater than f_i, the ion plasma frequency (such as at $f = 13.56$ MHz), the sheath is not influenced by the periodic variation of the biasing voltage.[33] When a positive ion diffuses from the plasma bulk into the sheath region, it will then be accelerated toward the substrate, which it strikes with a maximum kinetic energy $E_{i,\max}$[32]

$$E_{i,\max} \sim e|V_p - V_B| \equiv eV_{\rm sh}. \tag{3}$$

In the pressure range generally used for plasma processing, however, the ions lose part of their energy due to elastic, inelastic, and charge transfer collisions in the sheath and they exhibit an ion energy distribution function (IEDF). Typical shapes of the IEDFs obtained on grounded or biased surfaces in continuous or pulsed rf, MW, and MW/rf plasmas are shown in Fig. 4.

Appropriate control of ion bombardment energy ($E_i < 1$ keV) is particularly important in the context of etching and deposition of thin films at low substrate temperature T_s. Film growth under simultaneous ion bombardment leads to growth-related effects such as interfacial atom mixing, high surface mobility (diffusion) of deposited species, resputtering of loosely bound species, and deeper penetration of ions below the surface, leading to the displacement of atoms (forward sputtering or knock-in effects).[34,35] Such phenomena lead to the disruption of growth nuclei, to the suppression of columnar structure, and hence to material densification. Such processes can be well described by the structure zone model, first proposed for metals by Movchan and Demchishin,[36] and further developed by Thornton,[37] before its revision for PECVD by Messier *et al.*[38,39] The latter authors showed that T_s required for obtaining high film packing density can be decreased by superimposed ion bombardment, due to the effects mentioned above. This has since been clearly demonstrated for sputtered[40] as well as PECVD[41] optical films. A recent new structure-zone model also includes the flux of energetic particles as one of the key parameters.[42]

Different approaches have been used to quantitatively describe the ion bombardment, from which it appears that a key parameter for describing such effects is the energy E_p delivered to the growing film per deposited particle[43]

$$E_{p(T_s=\mathrm{const})} = \frac{E_i\phi_i + E_n\phi_n}{\phi_m + \phi_r} \sim E_i\frac{\phi_i}{\phi_m}, \tag{4}$$

where E denotes energy, ϕ the particle flux, and the indices i, n, m, and r refer to ions, neutrals, condensing precursor species, and trapped inert gas, respectively. As a first approximation one can neglect ϕ_r against ϕ_m and $E_n\phi_n$ against $E_i\phi_i$, and obtain the simplified relation in Eq. (4). Such approximation is clearly possible in ion beam experiments; however, the energy flux of neutral particles may become significant in PECVD, since a certain fraction of the initially accelerated ions become neutral due to charge transfer collisions in the sheath region. Detection of neutral species and determination of their energy is difficult and requires careful measurements involving mass spectrometry combined with ion energy analysis.[44,45]

The systems applied for PECVD of optical films and coatings are schematically illustrated in Fig. 3, and may be distinguished based on the level of control of the bulk plasma characteristics and ion bombardment effects. The rf systems depicted in Figs. 3(a) and 3(b) are similar to those frequently used in microelectronics industry for PECVD and reactive ion etching (RIE).[35,46] The deposition rates on the grounded electrode are substantially lower than on the rf-powered electrode (usually 5–10 times). Relatively high E_i values on the powered electrode at $T_s \sim 25$ °C lead to high film index, density, hardness, and stress (see Sec. IV). In rf discharges the dissociation rate in the gas phase may be insufficient, often resulting in increased optical absorption due to substoichiometric composition. Typically, $V_p \sim 20$ V, leading to $E_{i,\max} \sim 25$ eV on the grounded electrode [see Eq. (3) and Fig.

4(a)]. On the rf-powered electrode, the E_i values may reach several hundred volts; however, ϕ_i is low and may lead to a high film compressive stress (σ_-).

Most successful systems for optical coatings are based on MW plasma [Figs. 3(c)–3(h)]. In a single-mode MW reactor [Fig. 3(c)], the substrate is placed on a grounded or floating substrate holder, facing a MW (low water content fused silica) window through which the MW power is supplied by different devices such as linear or horn antennas [Figs. 3(c) and 3(d)], or standing or traveling wave (slow wave) applicators [Fig. 3(f)]. The V_p values are typically around 10 V, generally yielding $E_i \sim 5-10\,\mathrm{eV}$ such as in the continuous wave (cw) mode [Fig. 4(b)] (for a review see, for example, Refs. 20, 26 and 47).

Returning to Eq. (4), it appears desirable to maintain the E_i value relatively low (sufficient for film densification), while increasing the flux ratio ϕ_i/ϕ_m. This implies that an independent or selective control of ($E_i, \phi_i/\phi_m$) and of the bulk plasma processes is needed. This is impossible in conventional cw plasma reactors, which use a single power source to excite the discharge. However, two approaches to obtain selectivity have been explored: (i) pulsed-mode discharges and (ii) rf-induced surface biasing. When the MW power is pulsed, two plasma regimes can be distinguished during each pulse cycle: a high density plasma during the ''T_{on}'' period; and a decaying plasma during the ''T_{off}'' period. As a consequence, the IEDF adopts a bimodal shape [see Fig. 4(c)], with the high-energy peak corresponding to ions generated during the T_{on} period, and the low-energy peak being due to ions arising from the T_{off} period.[45] The ratio of the peak intensities depends on the duty cycle $D = T_{\mathrm{on}}/(T_{\mathrm{on}}+T_{\mathrm{off}})$ which, in turn, enables one to further tune the plasma–surface interactions in deposition, etching, or surface modification processes.

Pulsed MW plasma with low pulsing frequency, $f_p = 1/(T_{\mathrm{on}}+T_{\mathrm{off}}) < 100\,\mathrm{Hz}$, and a low duty cycle, $D<0.2$, have become prominent for optical and functional coatings:[20,45,48] On the one hand, high power during the T_{on} period leads to high n_e, ϕ_i, and dissociation rate values, and hence to a high process rate; on the other hand, longer T_{off} periods allow more time for the precursor gas to fill the volume in front of the substrate, thus leading to an enhanced film uniformity. This process has achieved the highest level of sophistication at Schott Glaswerke GmbH [Mainz, Germany; see Fig. 3(e)].[19,20] In their so-called plasma impulse CVD (PICVD) process, the dielectric substrates are placed directly on the MW window; in such a case, at a relatively high pressure on the order of 1 Torr, a very dense plasma is formed in front of the substrate during a very short pulse (typically 1–100 ms in duration). During the T_{off} period, enough time is allowed for replenishment of the working gas, done within several tens of milliseconds. Very high deposition rates (5–15 nm/s) and good uniformity, <1.5% variation over ~90 mm diameter, have been reported. The good uniformity obtained is attributed to the complete reaction of the working gas during the pulses.[19] Using the substrate as a MW window decreases the need for cleaning the reactor walls and the window itself; in addition, different shapes can be uniformly coated, such as plane disks, dome shapes, tubes, rods, lenses, etc.

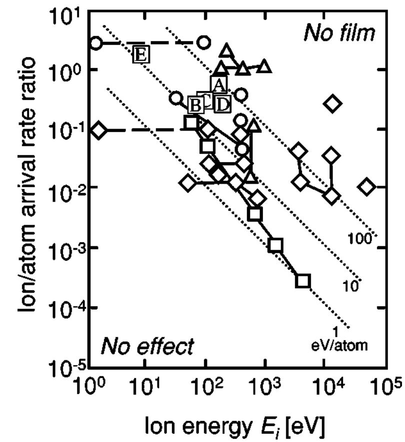

FIG. 5. Plot of critical ion/condensing particle arrival rate ratios $(\phi_i/\phi_m)_c$ vs critical ion energy $(E_i)_c$, required for film structural modification, particularly densification: (A) $SiN_{1.3}$:H, (B) SiO_2:H, (C) a-C:H, (D) TiO_2 obtained from MW/rf plasma, (E) estimated for TiO_2 based on the data in Ref. 20. Other data points are from Ref. 40 for different materials obtained by PVD techniques: (○) SiO_2, (△) other dielectrics, (□) metals, (◇) semiconductors (modified after Ref. 41).

A dual-mode microwave/radiofrequency (MW/rf) plasma approach has been developed at École Polytechnique in Montréal[41,48,49] [see Fig. 3(f)]. The substrates are placed on the rf-powered substrate holder facing the MW window, through which the MW power is applied using a linear slow wave applicator. The latter has a typical length of 20–30 cm, but even larger industrial-size versions (e.g., 1.5 m) have been designed and patented;[50] other applicators, e.g., slotted waveguides and surface wave launchers[26,47] have been considered and tested. The possibility of selectively controlling E_i and ϕ_i values is illustrated in Figs. 4(d) and 4(e). Other concepts include a remote MW/rf design[51,52] [Fig. 3(g)] and electron cyclotron resonance (ECR) configurations [e.g., distributed ECR (DECR)[53] or integrated distributed ECR[54]], in which a magnetic field is applied in conjunction with the MW discharge in order to further increase the dissociation rate and n_e, but at lower pressures ($\leq 10^{-3}$ Torr) [see Figs. 3(e) and 3(h)].[55,56]

It has been proposed that critical ion energies $E_{i,c}$ and critical ion flux ratios $(\phi_i/\phi_m)_c$ exist, which can be associated with transitions in the evolution of film microstructure and properties.[38,40,41] Clearly, E_p in Eq. (4) can be adjusted to the same level by combining low and high E_i and ϕ_i/ϕ_m values. However, experience suggests that good-quality (dense, hard, chemically stable, low stress) films are preferably deposited under conditions of low (10–30 eV) or intermediate (~100 eV) ion energies, sufficient for densification ($E_i \sim E_{i,c}$), but using high ϕ_i. This reduces the microstructural damage and gas entrapment, generally yielding low σ values. High fluxes are very advantageous, especially when one aims to achieve high deposition rates (>10 nm/s).

In Fig. 5 we show a comparison of our own results for SiO_2:H, $SiN_{1.3}$:H, TiO_2, and a-C:H films with the compila-

tion of literature data by Harper *et al.*,[40] who have summarized examples of $E_{i,c}$ and $(\phi_i/\phi_m)_c$ values reported to be necessary for property modification in numerous materials deposited by different (non-PECVD) ion-assisted techniques. One should note that the $E_{i,c}$ values are lower and $(\phi_i/\phi_m)_c$ values are higher for the MW and MW/rf PECVD data than most of the other results. The energetic conditions leading to good-quality optical films obtained by the PICVD process also fall within the same energy limits, namely low ion energy ($E_i \leqslant 10\,\text{eV}$) but high (ϕ_i/ϕ_m) values $[(\phi_i/\phi_m) \sim 1-10]$, due to a high power density and ionization rate.[20]

Different precursor gases can be used to fabricate optical films possessing (arbitrarily) low ($n_L < 1.5$), high ($n_H > 1.8$), and medium ($n_M \sim 1.5-1.8$) refractive indices (see Fig. 2 and Table I). The choice of starting materials and the corresponding characteristics of the optical films obtained are discussed in Sec. III.

III. OPTICAL PROPERTIES OF PLASMA-DEPOSITED OPTICAL MATERIALS

A. Optical characterization methods

Very often, optical characteristics of PECVD films reported in the literature are incomplete: in many cases, n values are given without referring to wavelength, and they are not accompanied by k, and the models used for the determination of n and k are not sufficiently described. In this section, we give a brief overview of approaches which should be taken into account.

Usually, optical properties are determined either from spectrophotometric (reflectance R and/or transmittance T) or ellipsometric measurements, among which variable angle spectroellipsometry (SE) or (VASE) combined with R and T measurements appear to be most powerful. Ellipsometry deals with determination of relative phase change of a reflected polarized light beam as opposed to absolute intensity measurements in spectrophotometry, making it more sensitive to very small changes in the optical properties at the surface of the sampled material. Spectrophotometry is more appropriate when evaluating the performance of a coating system such as an optical filter. For ''postprocess characterization'' of complex optical coatings (sometime called ''reverse engineering''), both methods share the same difficulties, related to the models used for reproducing the measured data, and the optimization algorithms used.

The most widely used dispersion models are the semiclassical Sellmeier and Cauchy relations for $n(\lambda)$,[57] and the Urbach tail relation for $k(\lambda)$.[58] Lately, new dispersion relations such as the Forouhi–Bloomer[59,60] and the Tauc–Lorentz formulæ,[61] based on a simplified expression for k from allowed electronic transitions in solids, have been shown to work well with plasma-deposited optical materials.

Effective medium approximation (EMA) models are frequently applied to account for index inhomogeneities, and to estimate the porosity or other microstructural features in the materials.[62–64] They may also be convenient for describing $n(z)$ in graded-index films;[65,66] $n(z)$ being formulated as a function of the volume fraction only, with no need to refer to the wavelength.[66] The use of EMA is justified only when the material's inhomogeneities are much smaller than the wavelength of the probing light ($<\lambda/10$).[67] Bruggeman EMA is used for a heterogenous medium with components of small size randomly distributed, while the Maxwell–Garnett model is more appropriate when one of the components surrounds the others and acts as a host material.[68] Components of the EMA models must be chosen with care to reflect the real composition of the material (sometimes including voids, or an optically absorbing phase, such as a-Si). However, one could question the utility of Maxwell–Garnett and Bruggeman EMA when the inhomogeneity is on the atomic scale; this applies to ''solid solutions'' such as SiO_xN_y, or when dopants and impurities are present (H, F, Cl, C, etc.) (see the discussion in Ref. 69), in which cases no particular phases with a bulk dielectric response can be identified.[70] For those materials, Bruggeman EMA can be a practical way for modeling n and k, but it cannot provide precise information relative to the composition and structure; this requires more complex EMA models, dealing directly with the identity of polarizable elements and their number per unit volume (the tetrahedron model is an example). Small surface roughness can be adequately modeled using a surface EMA layer with a 25%–50% air content;[71] this approach considers only the effect of roughness on n at the surface, and not the loss of light by scattering, the latter being hidden in the absorption term.

Simpler relationships between n and the density ρ, such as Lorentz–Lorenz $[(n^2-1)/(n^2+1)=4\pi/3\Sigma_j f_j \alpha_j]$ and Gladstone–Dale $[\rho=k_1(n-1)]$ relations, are sometimes used in order to elucidate the effect of deposition technique on n (here, f_j and α_j are the volume fraction and the polarizability of each component, and k_1 is a constant).[72] Clearly, such relations can help to predict and compare optical properties of films deposited using different fabrication parameters (sometimes referring to the concept of molar refractivity, which works perfectly with gases, and leads to rough approximations with solids[73]) but, once again, small quantities of ''impurities'' that lead to substantial changes in n and k are not considered by such simple relations.[74]

Reliable determination of the optical properties is generally based on the optimization (mostly nonglobal optimization). In such situations, it is very important to have a good starting ''guess'' for *n, k*, and the thickness d. In the case of single layer films with no *a priori* knowledge of n and k, the optical characteristics can also be obtained from envelope methods that provide analytical expressions (under several assumptions) for the parameters (*n, k, d*) as a function of T[75–77] or R.[78]

Using SE or T and R data, it is difficult to determine small k values below 10^{-4} (absorbance $A < 0.1\%$). Here, the use of photothermal deflection spectroscopy or mirage effect is more precise.[79,80] In these very sensitive methods, a deflection angle as small as 10^{-10} rad can be detected, which corresponds to $k \sim 1.6\times10^{-10}$.

Optical characterization is particularly critical in the case of inhomogeneous optical films. On the one hand, we con-

sider ''accidental'' inhomogeneities as a nondeliberate consequence of the fabrication process; these include: (i) fluctuation of the plasma parameters during the deposition process, (ii) surface and interface roughness, and (iii) formation of a physically thick interfacial region (or ''interphase'' [81]) due to specific plasma–surface interactions such as vacuum ultraviolet (VUV) radiation crosslinking and interface mixing when polymer substrates are employed (see Secs. III and IV). On the other hand, deliberate inhomogeneities are obtained by either: (i) continuous variation of plasma parameters (for example, gas composition or substrate potential), such as in the fabrication of rugate filters or graded index devices (see Sec. V), or (ii) doping the PECVD matrix material with clusters of another medium (for example, metals or semiconductors), in order to obtain nanocomposite films (see Sec. III B 9).

For characterizing inhomogeneous optical films, three different *ex situ* approaches can be applied: (i) analytical methods considering specific simplifications [such as the Wrentzel–Kramers–Brillouin–Jeffries (WKBJ) approximation] and small inhomogeneities;[82] (ii) discretization of the films into several homogeneous steps,[82] followed by numerical optimization; in this approach, a large number of fitting parameters introduces multiple solutions, and may lead to a large uncertainty in the results; (iii) numerical iterative methods such as Newton–Kantorovitch and Newton–Gauss, when one knows the thickness with high precision.[83]

The use of SE for the characterization of inhomogeneous films is discussed in more detail in Ref. 84. The characterization based on *in situ* measurements should, in principle, give more insight into the $n(z)$ profile. In fact, the problem still remains a difficult one, particularly when optimization is used, since multiple solutions may persist. Analytical solutions to the inverse problem can be used only for smooth variations of $n(z)$, when the WKBJ approach can be applied. Envelope methods using analytical expressions have been proposed for *in situ* T,[85] R,[86] and SE[87] measurements. A new method based on a higher-order WKBJ approximation and *in situ* SE appears most promising for both precise $n(z)$ determination, and for real-time monitoring[88] (see Sec. VI).

The following sections survey various plasma-deposited materials already introduced in Fig. 2, with their potential use in optical coatings. Table I gives a list of the optical properties and known precursors, and selected $n(\lambda)$ and $k(\lambda)$ dispersion curves are shown in Fig. 6.

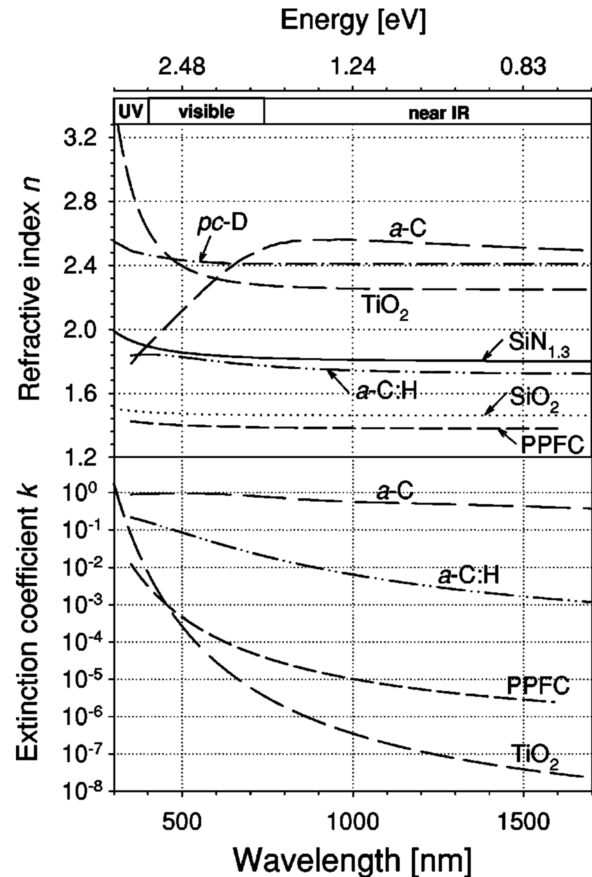

FIG. 6. Typical dispersion curves of different optical materials deposited by plasma [TiO_2, $SiN_{1.3}$, SiO_2 and PPFC: from our laboratory (École Polytechnique); diamond: after Palik (Ref. 281); *a*-C, and *a*-C:H: VASE software (Refs. 60 and 282)].

B. Transparent PECVD film materials

1. Silicon dioxide (silica, SiO_2:H)

Among all dielectric and silicon-compound materials, SiO_2 is probably the best-known low-index material (see Figs. 2 and 6). SiO_2:H is typically deposited from a mixture of SiH_4 and O_2. Its n value is usually higher than for the bulk or thermally grown oxide ($n \sim 1.459$).[89] Theoretical studies of the different phases of crystalline SiO_2 underline the link of n and optical gap E_g values to their structural characteristics. Early conclusions were that E_g and n correlate with the Si–O–Si mean bonding angle θ,[90] but more recent work also points to the importance of the crystal volume, density ρ,[91] and H incorporation.

In amorphous SiO_2:H, changes in θ values can be estimated experimentally from infrared (IR) spectra of the Si–O–Si stretching mode at 2260 cm^{-1}, with its peak frequency $\nu \propto \sin^2(\theta/2)$,[92] and its peak width being related to the θ distribution. A small θ value is related to stressed networks, mostly in dense structures; in such a case, the presence of three-membered rings in SiO_2:H is similar to the structure of bulk SiO_2 after heating beyond the melting point, followed by a sudden quench.[89]

Small-angle Si–O–Si bonds are very unstable; an accumulation of stress in the film can break these and force the network to relax, leading to a more flexible structure, accompanied by the formation of defect centers[93] or by reaction with water.[94] In fact, in the latter process, water absorption in pores,[95] may not necessarily be associated with aging, since not all types of pores give rise to water sorption. Martin *et al.*[96] have shown that there exist pores which considerably reduce n_{eff} without interacting with water, the film index being found to be the same in vacuum and in air. This leads to the concept of ''open'' or ''closed'' pores, and to their size.[97]

In SiO_2:H depositions from SiH_4/O_2 mixtures, the O_2 flow rate is typically twice that of silane, or more, depending on the plasma conditions and the dissociation rate. It is current to replace O_2 with nitrous oxide (N_2O), since the chemical bonds in N_2O break more easily in the gas phase, leading to higher deposition rate (activation energy $E_a = 2.5$ eV/molecule in N_2O,[98] compared to $E_a \sim 6.5$ eV/molecule for O_2).[99,100] The use of N_2O can introduce some N impurities into the oxide.[101] However, N concentration is usually less than 3 at. %, due to high affinity of Si with O, and even smaller with ion bombardment or heating. A 5% N concentration is enough to slightly affect the value of n ($\Delta n = 0.005$),[101] suitable for waveguide applications. Use of He has been shown to reduce the number of Si–H, Si–N, Si–OH, and N–H bonds in SiO_2 made from SiH_4/N_2O.[102]

SiO_2:H usually contains 5–15 at. % of hydrogen, mostly in the form of –OH, which has an effect on the optical properties and the stability of the material. Recent works have shown that during deposition from a SiH_4/O_2 mixture, the surface of the growing oxide is initially covered with silanol (SiOH) species,[103] due to instant oxidation of SiH_x (x depends on the dissociation level) by atomic oxygen. The SiH_x groups react further with SiOH and Si–O–Si to give H_2O and Si–O–SiH_x, which is oxidized by neutral O, leading to superficial–SiOH terminations. It is interesting to point out the effect of OH groups on the optical properties of SiO_2:H; OH passivates the material, so that practically no dangling bonds are detected in H-rich SiO_2:H. However, OH can react further with H_2O molecules that penetrate to the pores and change n. A network of Si–O–Si bonds is relaxed and more flexible if it contains a high OH content.[93] The presence of OH can also ''stabilize'' low-angle Si–O–Si bonds in disordered structures that would otherwise relax during the growth, giving rise to a decrease of the mean θ, and to an increase of compressive stress σ_-, ρ, and n.[104]

Deposits without heating possess higher n ($\sim$1.485)[89] than when annealed: annealing (at over 250 °C) and O_2^+ or Ar^+ bombardment assist desorption of weakly bonded and isolated OH and reactions of H-bonded superficial OH groups, resulting in the formation of H_2O (thermally or ion-assisted desorbed) and Si–O–Si, and in an increased number of O vacancies. The width of the Si–O–Si IR absorption peak decreases, which is related to narrowing of the θ distribution. Simultaneously, ν shifts toward higher frequencies, due to an increase of θ, and hence smaller Si/Si distance [$d_{si/si} \propto 1/\sin(\theta/2)$],[92] which still remains smaller than in thermal oxide.[105] O_2^+ bombardment seems to be particularly efficient for reducing H concentration in the film.[103,106] When dissociation of SiH_4 is high, Si exists on the surface, and it is easily oxidized, compared with SiH_2 and SiH_3 groups, for which several reactions with oxygen are needed to release all H atoms: this means that higher plasma density (high power) can reduce H concentration, such as in ECR,[104] MW, or MW/rf[41] plasmas. Except for Si-rich oxides, no Si–H bonds are usually detected.[103]

An important problem with silane as a precursor is the formation of particles. Silane can react with traces of humidity in the gas line and form powder that can reach the chamber, and clog valves and mass flow controllers; thus, it is essential to purge the lines periodically and keep them clean. In the plasma, silane produces reactive radicals that can react rapidly in the gas phase, forming particles, and resulting in the presence of nodules and large voids in the films, which change n_{eff} and cause scattering losses. Several steps can help to solve this problem; namely: (i) reduced operating pressure, such as in the ECR plasma; (ii) dilution of SiH_4 in argon or helium; (iii) heating the electrode;[107] and (iv) use of a pulsed discharge.[108,109]

The use of organic precursors instead of SiH_4 is motivated by its hazards, since SiH_4 is strongly pyrophoric, and by the fact that SiH_4 leads to low surface coverage, due to its low surface mobility. For the deposition of SiO_2-like PPOS, TEOS is widely used, sometimes mixed with O_2. Other frequent precursors are HMDSO and TMDSO (see Table I). Most popular organic precursors are liquid and require the use of a bubbler (see theoretical study in Ref. 110) or a liquid injection system.

With TEOS, the reaction occurs on the substrate surface, while chamber walls can be maintained at 45 °C to prevent extensive deposition on walls and particulate formation.[111] At low temperature (<200 °C) and no significant ion bombardment, absorbed TEOS reacts incompletely with O_2, which results in porous films, with a high concentration of OH and CH groups, unstable in ambient air. At 200 °C, the CH is removed and less but still some isolated OH and CO groups appear as a product of TEOS oxidation: therefore SiOH, as well as H_2O, are intermediate products that react further to deposit SiO_2; at low working pressure, OH can react and desorb without being incorporated into the film.

Plasma-polymerized SiO_2:H:C films from the HMDSO possess n values ranging from 1.45 to 1.55, depending on the deposition conditions.[112] Interpretation of the value of n can be complex: C- or Si-rich films exhibit higher n (and k), while higher porosity or attached OH groups lead to a reduction of n.[113] Film microhardness can be increased by adding CH_3 groups using methanol in the feed stream; as a result, k also increases.[114] O_2-rich gas mixtures are used to keep the carbon concentration low.[115] Noble gases, Ar or He, are sometimes added, and higher power plasma density is applied to enhance fragmentation in the gas phase, to reduce the organic content (CH_2 and CH_3 radicals) in the films.[112]

2. Silicon nitride ($SiN_{1.3}$:H)

Several nitride materials are transparent; although AlN and BN may be used in the near future for various multifunctional coatings, $SiN_{1.3}$ is probably the only one used for its optical properties. So far, the use of nitrides in optical coatings has been limited due to a difficulty in forming transparent, good-quality layers by evaporation or sputtering in the presence of N_2.[116]

Silicon nitride can be deposited by PECVD using SiH_4 mixed with nitrogen (N_2) or ammonia (NH_3), while the use of organosilicone precursors is mainly limited by the pres-

ence of carbon. The n values reported for PECVD $SiN_{1.3}$:H vary from about 1.65 to 2.05 (Fig. 2), depending mainly on the film microstructure and composition.

When deposited at low temperature and low energy conditions, $SiN_{1.3}$:H exhibits columnar structure; therefore, more energy must be brought to the surface (by ion bombardment or substrate heating) in order to achieve high packing density. The residual gas concentration in the chamber must also be kept low, as $SiN_{1.3}$ can react rapidly with traces of O_2 or H_2O, thereby lowering its refractive index.[117,118] García *et al.*[119] reported that an atomic percentage of oxygen as low as 3% in $SiN_{1.3}$ can lead to a decrease of n from 1.99 to 1.85.

The major ''impurity'' in $SiN_{1.3}$:H, of course, is hydrogen, which has a significant impact on the electronic and optical properties. Due to its dense structure and the valence of nitrogen versus oxygen, the amount of H (passivating broken bonds) is substantially higher in the nitride than in the oxide,[41,120] and it mainly appears in Si–H and N–H bonds. Replacing Si–N by Si–H has little effect on the gap [$E_g = 5.3$ eV (234 nm) for H-free $SiN_{1.3}$],[121] but N–H bonds considerably reduce the n value: In fact, energy band calculations for silicon diimide [$Si(NH)_2$], which can represent the NH-saturated form of $SiN_{1.3}$:H, predict gap values between $E_g = 6.4$ eV (195 nm) and $E_g = 6.17$ eV, with $n = 1.69$ and $\rho = 1.98$ g/cm^3 (compared to 2.08 g/cm^3 for stoichiometric Si_3N_4).[121,122] For silicon-rich nitride, Si–H replaces Si–Si bonds, an approach used for tailoring the valence edge and increasing E_g.

A decrease of n with NH incorporation has frequently been observed experimentally.[123–125] This is often attributed to passivation of dangling Si bonds on the surface to form N–H, which leads to disruption of the network, $Si(NH)_2$ incorporation, and to a higher void fraction.[125] The reasons for the preferential bonding to N instead of Si, forming –NH groups, is attributed to the fact that –NH (with two valence electrons) is easier to coordinate in an amorphous network than N (with three valence electrons).[120] The analysis of n is often performed by using simple EMA models, mixing bulk Si_3N_4 with voids: A decrease of n due to NH incorporation and lower Si–N and Si–Si bond concentrations is then masked in an ''effective void fraction,'' which is unrelated to real voids.[125] Lower n values due to hydrogen were demonstrated by using more accurate tetrahedron optical models,[67,122] which resulted in smaller values of void fraction (<6%).[123,126] Multitechnique analysis[127] has suggested that $SiN_{1.3}$:H should be considered as a solid solution of $SiN_{1.3}$ and $Si(NH)_2$.

The highest n value can possibly be obtained for H-free nitride. According to Smith,[120] one way to accomplish that with SiH_4 precursors is to precisely control the gas flow rate in the chamber: since H reacts preferentially with excess N,[123] one should reduce the amount of NH_3 (or N_2) to a critical point (for example using mass spectrometry), so as to obtain stoichiometric $SiN_{1.3}$. Hofrichter *et al.*[128] succeeded in reducing [H] from 25% to 9% (increasing n from 1.74 to 1.96) by decreasing SiH_4 flow rate and total working pressure (probably linked to small values of SiH_4 residence time) in a ECR plasma reactor using $SiH_4/N_2/O_2$ gas mixture.

One can also reduce [H] by annealing; however, to remove hydrogen from the N–H bonds, temperatures above 900 °C are required.[129]

Another way to avoid hydrogen incorporation is to use silicon halide precursors, such as $SiCl_4$ or SiF_4.[130] Chemical affinity between Cl atoms and H atoms promotes the formation of HCl, which can further reduce the H concentration. In addition, the presence of halogen atoms gives rise to a competitive etching process during deposition, which can reduce the film roughness.

For $SiN_{1.3}$:H films grown in MW/rf plasma at $T_s \sim 25$ °C, controlled ion bombardment gave rise to n values between 1.65 and 1.90 for bias values of ''0'' and 800 V, respectively.[131] The resulting hydrogen concentration was found to vary between 12 and 16 at. %, systematically less than in a pure rf discharge.[41] It has been proposed that some of the hydrogen is not chemically bonded, but is chemisorbed on inner surfaces.[41]

Attempts have been reported to deposit ''nitride-like'' $SiN_{1.3}$:H:C films using organosilicone precursors. The use of HMDSN and HMCTSZN,[132,133] mixed with N_2 or NH_3, resulted in n values strongly depending on the gas mixture and other deposition parameters, such as the pressure and V_B. Frequently, C-rich and Si-rich films are deposited, yielding an n value of 1.8 at the expense of higher k.[133]

3. Titanium dioxide (titania, TiO_2)

Since the highest refractive index of $SiN_{1.3}$ above 2.00 can be achieved only with difficulties, the search for high n materials is of constant importance. Among these, titanium dioxide (TiO_2) attracts the most attention, due to its high ionic character and n values exceeding 2.25. The reason for its high index resides in the TiO_6 octahedral structure, the building block of rutile and anatase. The n values reported in the literature for non-PECVD TiO_2 vary from 1.79[134] to 2.6.[135]

The deposition of oxides of transition metals such as Ti and Ta is complicated by the fact that they can take different forms and stoichiometries, some of which are nontransparent (e.g., TiO or Ti_2O_3).[136] In addition, in the case of TiO_2, three stable crystalline phases are possible: rutile, anatase, and brookite. Rutile, with the highest density, is the most desired phase in terms of transparency and index value, but it also has the highest birefringence, with $n_0 = 2.9$ and $n_e = 2.6$, and is often undesired in term of scattering: anatase, which differs from rutile in the coordination number of its TiO_6 octahedra (10 in the case of rutile, 8 for anatase), is less birefringent, and it has an index of 2.5; brookite, an unstable rhombohedral structure, is rarely observed in thin films (it has been deposited on soda-lime glass using sol–gel technique in presence of Na).[137]

The most frequently used precursors for plasma deposition of TiO_2 are $TiCl_4$ (mixed with O_2),[138–140] TIPT,[141,142] TEOT,[143] $Ti(O-i-C_3H_7)_4$,[144,145] and $Ti[OCH(CH_3)_2]_4$[146] (see Table I). The use of metalorganic precursors has been

stimulated by two considerations: (i) $TiCl_4$ is hazardous, highly corrosive, and it requires special installations; and (ii) Cl can be a major contaminant in TiO_2 and increase its absorption coefficient.[138,141]

Both rutile and anatase are tetragonal and they often coexist in the films. High temperatures and ion bombardment energy may be needed during growth to control the rutile/anatase concentration ratio. At temperatures below 200 °C, anatase is frequently observed, and it contributes to lower n. Using a $TiCl_4/He/O_2$ mixture in an ECR/rf PECVD system, Lee[147] observed that rutile is usually formed above 600 °C, and that it is the only phase observed above 900 °C. For higher energy of the bombarding ions, they observed a lower deposition rate, resulting from RIE due to Cl competing with film densification. However, anatase is favored at high V_B values. For most applications, the crystallization of the films and the size of the crystallites must be carefully controlled, as it can give rise to light scattering. Temperature is often kept below 200 °C to prevent crystallites formation. The crystallization and phase change temperatures vary with film thickness,[148] impurities,[149] and composition of the glass substrate.[150] The room-temperature deposited films generally possess a low concentration of Cl (5%–10%), which further decreases with increasing T_s and V_B,[140] accompanied by an increase of n from 2.25 to 2.40. The films often exhibit excess oxygen content (O/Ti>2), related to hydroxyl groups and film density, which affects the n value; this has also been reported for sputtered TiO_2 layers.[151]

4. Aluminum oxide (Al_2O_3)

Aluminum oxide (Al_2O_3), frequently used as a medium-index material ($n \sim 1.62$), is rarely prepared by plasma for optical coatings. It can be deposited using $AlBr_3$,[152] $AlCl_3$, TMA,[153] or TMAA[154] precursors, mixed with O_2 or N_2O (see Table I). $AlCl_3$ reacts violently with moisture, producing heat and HCl vapors; it thus requires particular care. TMAA results in less carbon incorporation in the deposited layer, compared to TMA.[154] Recently, Chryssou[155] demonstrated that Er^{3+}-doped Al_2O_3 can be fabricated by plasma, using $Er(thd)_3$ as the erbium precursor.

5. Tantalum pentoxide (Ta_2O_5)

Considerably less work has been reported for PECVD of Ta_2O_5. Its index was found between 2.12 and 2.16 (at 632.8 nm).[156] The precursors used for its deposition are organometallics, such as $Ta(OC_2H_5)_5$ and $Ta(OCH_3)_5$, and halides (TaF_5), mixed with O_2 (see Table I).

6. Fluorinated silicon dioxide (SiO_2:F or SiOF)

Complementary to the work on high n materials, considerable effort has been devoted to the fabrication of low n films, namely the fluorine-doped silicon dioxide (SiO_2:F, often called "SiOF"), giving rise to n between 1.41 and 1.43 (Fig. 2). This activity was mainly stimulated by its potential use as a low-permittivity (ϵ) material for intermetallic dielectric layers, to reduce the parasitic capacitance in multilevel interconnect microelectronic devices. The use of fluorine arose from low-ϵ properties of fluoropolymers and abundant literature on fluorine-doped a-Si, in which fluorine exhibits a stabilizing effect; it passivates dangling bonds, and reduces the hydrogen content. Many methods involving plasma have been applied to fabricate SiOF, using different organic and inorganic precursors; most frequent are the following: $TEOS/C_2F_6$,[157] $TEOS/O_2/CF_4$,[158] $TEOS/O_2/C_2F_6$[159–161] (or with He),[162] $SiH_4/O_2/CF_4$,[163] $SiH_4/N_2O/SiF_4$,[159] $SiH_4/N_2O/SiH_2F_2$,[159] $SiH_4/SiF_4/O_2$,[164] (or with Ar),[165] $SiH_4/N_2O/CF_4$,[166] FTES,[167] and $FTES/O_2/Ar$[168] (see Table I).

The reasons for the low-ϵ properties of SiOF are still under debate; this characteristic is usually attributed to ionic bonding contributions, such as the change in Si–O bond strength in the neighboring Si(O–)F sites, or replacement of–OH bonds in its structure. A reduction of n has also been observed in the visible frequency range, associated with a relaxation of the Si–O–Si bond angle θ, lower density, and shorter Si/Si interatomic distance,[158,162,169] at low [F] values, and with voids formation, especially for high [F] values.[169] Most of the fluorine atoms in SiOF with low [F] exist in the form of Si–F groups, which are formed by breaking distorted low-θ Si–O–Si bonds. PECVD SiO_2 films are known to exhibit a small-ring structure,[89] distorted in order to accommodate a bonding angle as low as 130°,[158] in comparison to ~147° for stable (bulk) SiO_2. When doped with fluorine, some of the rings are removed, the structure is relaxed, and θ increases to 146°–148°, and its distribution becomes narrower.[158,169] Less distortion leads to lower ρ and lower n in the visible and NIR.[169] In fact, a decrease of E_g with F incorporation has been observed, in agreement with reported linear correlation between θ and E_g obtained from band structure and density of states calculations.[90]

Another factor important for fluorine concentrations above 8 at. % is the formation of voids, which leads to lower n values.[169] As stated above, the replacement of O (divalent) by F (monovalent) atoms increases the concentration of terminations in the Si–O–Si network. With larger [F], the number of $Si(O–)_2F_2$ and $Si(O–)F_3$ sites increases, rendering the network more open and increasing the pore size.[162] However, in contact with ambient atmosphere, $Si(O–)_2F_2$ and $Si(O–)F_3$ sites are hydrophilic and they can react with water vapor, producing Si–OH bonds and HF, which does not desorb at temperatures below 250 °C.[162] Such water sorption and the creation of Si–OH sites in the case of high [F] values increases n from about 1.38 to 1.42.[157]

Based on the above, the key issue in SiOF films fabrication is to increase θ to about 148° without forming $Si(O–)_2F_2$ and voids. Depositions using high O_2 (or N_2O) concentrations were found to densify the films and to incorporate more F, effects attributed to higher O_2^+ bombardment.[159] Denison *et al.* reported stable SiOF with $n = 1.417$ and [F]=10.5 at. % obtained from high-density ECR plasma in a $SiH_4/SiF_4/O_2/Ar$ mixture.[165] The choice of precursor may also affect the concentration of weak $Si(O)F_2$ bonds in the film: for example, FTES has a direct Si–F bond which is

presumably stronger than its other bonds (Si–O, C–C, and C–O). Use of this precursor has been shown to reduce moisture absorption, compared to TEOS/C_2F_6 films.[167]

SiOF represents an attractive low n material; dense, stable films with $n=1.41$ and [F]=12 at. % can be used in numerous applications, while porous, unstable films with $n=1.38$ and [F]=20 at. % should be combined with a dense barrier layer (e.g., $SiN_{1.3}$ or TiO_2) in multilayer systems.

7. Plasma polymerized fluorocarbons (PPFC)

The research on PPFC has mostly been stimulated by the prospect of obtaining low n and low ϵ values such as for polytetrafluoroethylene (PTFE) (for example, Dupont Teflon, with $n=1.35$) or, more recently, for amorphous fluorocarbons, such as Dupont Teflon AF2400 ($n=1.29$) or Teflon AF1600 ($n=1.31$).[170] There now exists abundant literature on the use of fluorocarbon plasmas for film deposition, and for anisotropic etching of silicon and silicon dioxide.[171] By suitably adjusting the experimental parameters, one can shift the plasma conditions from etching to deposition modes.[29] Different precursors have been explored for deposition, frequently leading to n values between 1.35 and 1.38; they include C_2F_4, C_2F_6, C_4F_8, C_3F_6, HFPO,[172] $C_2H_2F_4$, CH_2F_4, FAS,[173] and PFDCH[174] (Table I). Small dispersion and low index are generally attributed to a high concentration of CF_2 groups in the films. Plasma-deposited films usually contain a significant concentration of dangling bonds (estimated at 10^{18}–10^{20} spin cm^{-3}),[174] which can react with atmospheric oxygen or water vapor leading to the formation of C═O groups,[174,175] and to aging effects.[176] Pulsed PECVD has been shown to produce PPFC with lower concentrations of dangling bonds.[172] In general, the PPFC films are very hydrophobic and not easily compatible with high n layers in multilayer systems, due to adhesion problems. They are, however, good candidates for smudge-resistent top coats.[177]

8. Carbonaceous materials (plasma polymers, a-C:H, DLC, polycrystalline diamond)

A large number of materials obtained by PECVD from hydrocarbon gases or vapors have been studied for their possible use in optical coatings. Their refractive index typically ranges from 1.6 to 2.2, and their absorption is often not negligible in the visible region ($k\sim0.002$–0.8), but they are transparent in the infrared region. They are particularly attractive in combination with their advantageous mechanical characteristics, such as high hardness ($H\sim15$–40 GPa), low friction coefficient ($\mu\sim0.05$–0.15), and high scratch resistance (see Sec. IV). These film properties strongly depend on the microstructure (sp^2/sp^3 hybridization ratio) and the hydrogen concentration [H], which are, in turn, controlled by the fabrication conditions, namely the E_i and T_s values (numerous reviews exist on this subject, for example, Refs. 178–180).

Several categories of such organic PECVD films can be distinguished, but the various research groups use different nomenclatures, and the boundaries between such materials are rather arbitrary. This includes plasma polymers (E_i $\leqslant30$ eV, [H]>35 at. %, $n\sim1.6$), and hydrogenated amorphous carbon (a-C:H) or DLC, which itself can be either soft (''polymer-like'' a-C:H, $E_i\sim30$–60 eV, [H]~30 at. %, $n\sim1.6$–1.8), or hard (60 eV$\leqslant E_i\leqslant1$ keV, [H]~20 at. %, $n=1.8$–2.2, $E_g=1.3$–2.0 eV).

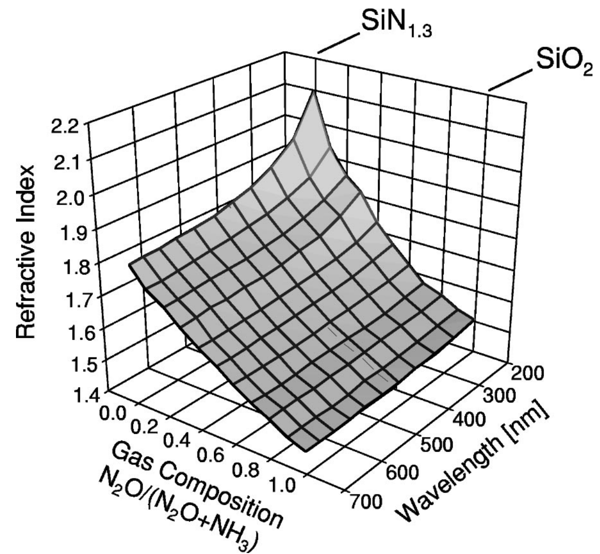

FIG. 7. Variation of the refractive index dispersion of SiO_xN_y rf-plasma-deposited at low temperature ($T_s\lesssim150$ °C) from $SiH_4/NH_3/N_2O$ mixtures.

In general, the characteristics of organic PECVD films depend to a lesser extent on the nature of starting hydrocarbon gas or vapor, but rather on the energetic conditions of the discharge. The resulting optical properties are related to hydrogen, which contributes to the formation of C–H σ bonds at the expense of π bonds (sp^2 hybridization), the latter ones affecting the density of states and E_g values.[180,178,181] The microstructure can be further influenced by doping a-C layers with nitrogen,[182–184] which can lead to higher k, higher conductivity (N acting as a dopant near the edge of the σ density-of-states in the sp^3 matrix), and to a higher Young modulus [N acting to promote three-dimensional (3D) curvature and attachment in the sp^2 clusters]; or with fluorine,[185] in order to obtain higher transparency.

Polycrystalline diamond (pc-D) films, with their high refractive index ($n=2.35$) and transparency over a very large wavelength range (0.2–20 μm), have also attracted much attention due to their extreme hardness ($H\sim90$–100 GPa) and chemical inertness (many reviews are available, for example Refs. 186 and 187). In the visible region, the optical use of diamond may be limited by light scattering on the relatively large crystals (~1 μm in size), and frequent incompatibility with traditional optical substrate materials due to typical T_s values in excess of 600 °C. However, very smooth, nanocrystalline diamond films[188] or laser-polished films[187] have been reported.

9. Inhomogeneous, graded-index materials

Several materials are particularly suitable for the fabrication of films with intermediate refractive indices and of in-

homogeneous (graded index) optical coatings, in which the refractive index profile $[n(z)]$ is continuously varied. This can be achieved by varying the gas composition,[131,189–192,128] or the film microstructure by controlling E_i.[131] The most extensively used material for this purpose is the amorphous hydrogenated silicon oxynitride (SiO_xN_y:H), obtained from gas mixtures with SiH_4. The n values depend on the nitriding versus oxidizing gas ratio (e.g., NH_3/N_2O or N_2/O_2, see Fig. 7). Since O has more affinity to Si than N, one can choose to control only the O_2 flow.[66] As for many other materials, the n value of SiO_xN_y:H strongly depends on [H] and T_s. In fact, the same n vs N_2O/NH_3 dependence has been obtained for films deposited in MW plasma at $E_i \sim 10$ eV and $T_s \sim 250$ °C as in MW/rf plasma at $E_i \sim 160$ eV and $T_s \sim 30$ °C,[131,193] clearly illustrating the beneficial role of ion bombardment, in agreement with the structure zone models.

Besides the n value, the deposition rate r_D has to be well controlled at every moment of the growth process of inhomogeneous coatings. Usually, r_D increases with O_2 concentration.[194] However, at conditions favorable for more pronounced gas phase reactions, such as at elevated pressure, the production of silica particles may compete with the film formation.[120]

According to the results of detailed SE and electron spin resonance measurements, SiO_xN_y:H films exhibit homogeneous and amorphous microstructures, close to those of a ''solid solution;''[195] no crystal formation has been observed up to a temperature of 900 °C. These measurements lead to certain limitations in the use of EMA approaches to derive structural characteristics of such films; the main concerns are as follows: (i) H incorporated in the films reduces n, which is difficult to account for in the EMA model;[195] (ii) films deposited at high E_i or T_s values represent solid solutions at the atomic level, containing O–Si–N bonds, hence no SiO_2 and $SiN_{1.3}$ domains can be distinguished; (iii) the optical characteristics may be shrouded by the presence of pores (possibly filled with water vapor), which result in lower n.

Other Si-based graded index materials have also been studied. These include GeO_2/SiO_2 films obtained from a TEOS/O_2 mixture doped with TMGe[196] (Table I). Their n values range from 1.463 to 1.477 for TMGe/TEOS ratios between 0% and 10%. Si-rich SiN_x:H (absorbing) films have been considered for NIR applications, benefitting from a change of n values from 3.1 (a-Si:H) to 1.72 ($SiN_{1.3}$:H).[190] Doping SiO_2 with F, leading to n values from 1.41 to 1.47, has also been studied for graded n applications.[160]

AlO_xN_y films obtained from $AlBr_3/H_2/N_2O/N_2$ mixtures have also been studied.[152] By controlling the N_2O/N_2 ratio, n ranged from 1.60 (Al_2O_3) to 2.10 (AlN), E_g varied between 5.1 and 7.0 eV, and optical transparency was >90%. The material possessed a crystalline AlN phase at low N_2O/N_2 ratios, while it was amorphous at high ratios. The crystallinity was attributed to energetic N_2^+ ions in the ECR plasma. X-ray photoelectron spectroscopy (XPS) analysis revealed a mixture of Al_2O_3 and AlN phases.

As already mentioned above, n of carbonaceous coatings can be varied over a wide range, namely from 1.6 to 2.2.

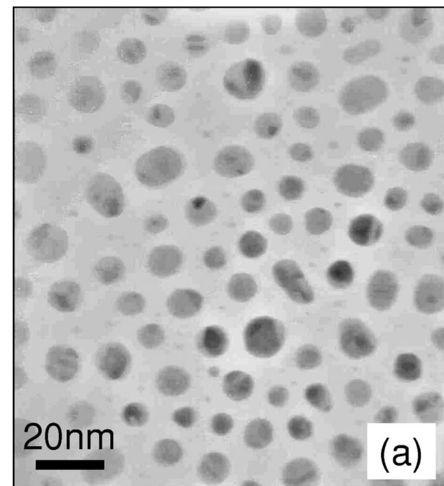

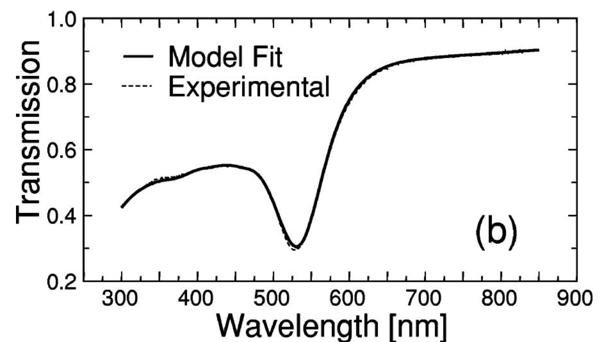

FIG. 8. Nanocomposite film formed by gold clusters in a SiO_xN_y matrix: (a) TEM micrograph; (b) measured and modeled transmission spectra, using a generalized Maxwell–Garnett model, (after Ref. 283).

This has been applied for wide-band AR coatings on Ge and ZnS in the NIR region.[197] Similarly, addition of O_2 to a hydrocarbon allowed one to vary n from 2.13 to 1.64.[198]

As already stated, variation of n in inhomogeneous coatings is based on changing the gas composition or the ion energy: as a consequence, the microstructure (particularly the porosity) may vary. Therefore, film stability and possible aging effects must be carefully assessed.

10. Nanocomposite films

The work on nanocomposite optical materials, formed by nanometer size (1–100 nm, mostly metal) particles embedded in dielectric matrices, has mainly been stimulated by new film properties such as optical selectivity (absorption filters; colored, decorative coatings; photothermal energy conversion) and optical nonlinearity. The former phenomenon is linked with the surface plasmon resonance.[199] Depending on the materials combination, particle concentration, their size, and shape, different colors can be obtained. In the latter case, the presence of nanoparticles leads to a substantial local field enhancement,[200] giving rise to third-order susceptibility $\chi^{(3)}$, up to 10^{-6} esu.[201–203]

The nanocomposite structures are usually fabricated by hybrid processes, combining PECVD of organic (PPFC, PPHC) or inorganic (SiO_2, Al_2O_3, $SiN_{1.3}$) matrices with si-

multaneous sputtering or evaporation of metals such as Au, Ag, Cu, and others (for more details, see Refs. 204 and 27).

Considerable effort has been devoted to analyzing the effect of microstructure on the properties of such nanocomposite materials [Fig. 8(a)]. In this respect, invaluable information can be obtained using EMA to interpret the SE, and *R* and *T* experimental data. In fact, using the generalized Maxwell–Garnett model, considering the permittivities of the host and the particle materials, the depolarization factor and the inter- and intraband electron transitions, the particle concentration, their size and shape can be obtained from noninvasive optical measurements [Fig. 8(b)].[205] Such a nondestructive approach may possibly also become invaluable as a structural characterization tool for ultrahard nanocomposite coatings and other materials described in a recent review.[206]

11. Exotic optical PECVD materials

Studies of novel ''exotic'' PECVD materials are stimulated by an attempt to combine optical with electrical and other effects. As an example, this group of materials includes transparent conductors such as indium–tin–oxide, obtained from indium nitrate pentahydrate and tin–chloride pentahydrate in water, using an ultrasonic nebulizer in combination with a rf ''mist'' Ar/O_2 plasma.[164] Conductive tin–oxide (SnO_2) films have also been fabricated.[207,208]

High-index chalcogenide glass films for NIR and IR applications, such as Ge_xSe_{1-x}:H, were fabricated from a H_2Se/GeH_4 mixture diluted in H_2 (85 vol. %) in an rf plasma at ambient temperature.[209] The *n* values varied from 2.56 for Se to 2.36 for *a*-$GeSe_2$. They were transparent in the 0.6–30 μm range, and they exhibit good mechanical and chemical properties (hardness, stress, adhesion, and water resistance). A decrease of *n* has been associated with higher [H]. For similar applications, silicon carbide (SiC:H) or mixed *a*-C:H/Si:H systems were studied.[210] The films fabricated in a capacitively coupled rf plasma exhibited high transparency above 500 nm, and the *n* values varied from 2.8 (*a*-C:H at $V_B=-200$ V) to $n=1.7$ (SiC:H at $V_B=-75$ V).

Mixed metal–oxide films were deposited from combined melted solid metal β-diketonates and liquid precursors by means of MW plasma metalorganic chemical vapor deposition[211] of yttria (Y_2O_3) stabilized zirconia (ZrO_2) (YSZ) from $Zr(acac)_4$ and $Y(dpm)_3$ (Table I). The transmittance of the films was found to be larger than 90%, with $n=2.1$. Additionally, barium titanate ($BaTiO_3$) and strontium titanate ($SrTiO_3$), which are known for their very high permittivities, were fabricated by combining melted $Ba(dpm)_2$ and $Sr(dpm)_2$ compounds (Table I) with TIPT in an O_2 plasma. The refractive index of $BaTiO_3$ and $SrTiO_3$ were both found to be 2.19 on SiO_2 substrates. The permittivity was estimated from capacitance–voltage curves to be 1×10^3 for $BaTiO_3$, and 1×10^2 for $SrTiO_3$, primarily due to a high ionic polarizability of these materials.

C. Effect of plasma on the optical properties of substrate materials

As already discussed in Sec. II, plasma is a rich source of energetic species such as ions, radicals, and photons, the latter covering the entire IR-VUV-soft x-ray region.[212] Therefore, energetic effects on the substrate materials are inevitable, especially when surface pretreatment for surface cleaning, activation, and modification becomes an integral part of the film fabrication process. Photons with energies from several eV to more than 20 eV can exceed those of covalent bonds, and they can penetrate deep into the material, depending on the absorption characteristics of the substrate.

In the case of glass, the effect of UV radiation has been shown to be less significant in fused silica or calcium fluoride, compared to multicomponent glass, such as BK7. In the latter material, the modified surface properties are attributed to the generation of electron–hole pairs and to trapping in different color centers associated with defects (vacancies, interstitial atoms, multivalent impurities, nonbridging oxygens, etc.),[213] and to ion migration towards the surface, giving rise to surface absorption. Annealing at 250 °C can reverse the effect of UV irradiation in some cases, depending on the types of color centers involved; however, surface absorption cannot be healed by annealing. Use of CeO_2-doped glass, in which the absorption bands are shifted to wavelengths higher than in the visible and UV ranges, can mask the effect of VUV radiation on transmittance.[214]

The effect of VUV irradiation is particularly significant in the case of polymers, such as PC, PE, and PMMA, since the photon energies exceed those of chemical bonds (for example, 3.2 eV for C–C, 3.6 eV for C–H, 4.2 eV for C–O),[215] and coincide with absorption bands in the near and far UV regions. The energetic photons can penetrate to depths of several hundreds of nanometers (20 nm at $\lambda=80$ nm, 1 μm at $\lambda=200$ nm) compared to bombarding ions which affect 1 or 2 monolayers. For these polymers, most frequently used in optical applications, degradation mechanisms include chain scissions, photo-Fries rearrangements, recombination of photolytic radicals, and photoinduced oxidation (when O_2 is present).[216] They contribute to crosslinking or branching, hence creating a denser top layer (about 50–100 nm thick), characterized by a slight increase of the near-surface *n* value (for example, $\Delta n\sim0.02$ in PC and $\Delta n\sim0.08$ in PET).[217] In many cases, VUV radiation can lead to photon-induced ablation (etching).[218] The absorption also depends on the type and concentration of additives (UV blocking agents, antioxidants, etc.),[219] which are designed to protect the polymer against UV, but which may enhance interaction with VUV in vacuum.

Interest in plasma–polymer interactions has particularly been stimulated by the use of plasma for adhesion improvement,[25,26] in which the VUV photons play an important role. Strong VUV radiation has been systematically studied for λ values above 100 nm,[218,220] in which the most effective appears to be the discharges containing H_2 (strong Lyman α line at 121 nm, and molecular bands), O_2 (strong resonant line at 130 nm), and He (intense line at 57 nm). In this context, one must take into account intense VUV features due to the excitation of impurities (fragments of

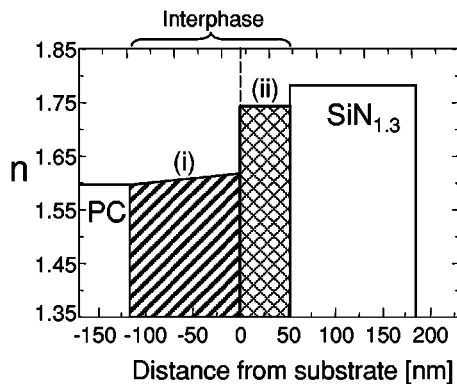

FIG. 9. Illustration of a structured interfacial region (interphase) between a plasma deposited film (here $SiN_{1.3}$:H) and a polymer substrate (PC). Schematic illustration of the $n(z)$ profile in the interfacial region shows: (i) a crosslinked layer formed by plasma pretreatment (attributed mainly to polymer interaction with energetic VUV emitted light), and (ii) a transition layer obtained after $SiN_{1.3}$:H deposition (modified after Ref. 217).

H_2, H_2O, hydrocarbons) desorbed from the chamber walls and from the polymer itself.[212]

Energetic interactions of plasma with the exposed polymer surface in the initial stage of the film growth lead to the formation of a physically thick, structured interfacial region (''interphase''), composed of a crosslinked layer followed by a transition layer formed by intermixing of the film and substrate materials, and possibly by voids[25,217,221] (Fig. 9). Using both noninvasive optical (*in situ* and *ex situ* ellipsometry, photometry) and invasive methods [elastic recoil detection, transmission electron microscopy (TEM), etc.], the interphase has been found to be 50–100 nm thick.[217,221–223] It plays a major role in the mechanical performance of films (see Sec. IV), and it should be included in the optical design (see Sec. V). *In situ* ellipsometry trajectory graphs reveal a graded layer at the interface also in the case of glass (nonpolymeric) substrates,[191] possibly related to the film nucleation process and porosity.

IV. MECHANICAL PROPERTIES OF PLASMA-DEPOSITED OPTICAL MATERIALS

The mechanical behavior of optical coatings is increasingly important, given the large variety of novel applications including adhesion to substrates such as polymers, mechanical stability, and integrity in ''hostile'' environments (e.g., humidity, temperature excursions, space, etc.), scratch, abrasion, and wear resistance, surface friction, hydrophobicity, hydrophilicity, etc. In this section, we give an overview of the mechanical properties of PECVD optical film materials, in particular of their intrinsic characteristics such as microhardness and stress, and adhesion to plastic substrates. Numerous mechanical testing methods have been reviewed (for example Refs. 24 and 224).

Hardness is an important ''active'' film property, which allows one to enhance the mechanical characteristics of the underlying substrate, such as resistance to mechanical intrusion, low friction, and others. Hardness may be defined as a resistance to local plastic deformation. Hardness tests, therefore, generally consist of pressing a hard indenter into the surface, and the appropriate hardness value H is obtained as

$$H = L/A, \tag{5}$$

where L is the applied load and A is the contact area.

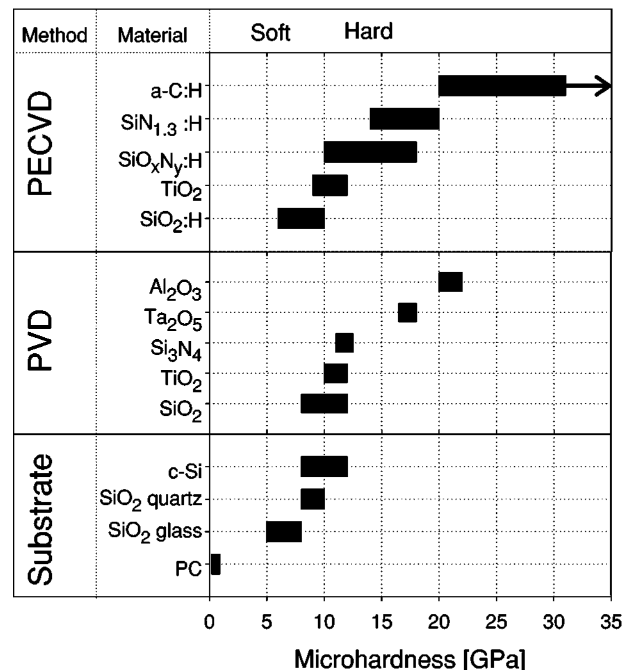

FIG. 10. Microhardness of different PECVD optical film materials; comparison with selected substrate and PVD materials.

In the case of optical coatings, the film thickness is typically below 1 μm, which makes it difficult to satisfy a general requirement to limit the indentation depth below 10%–20% of the film thickness, in order to avoid the influence of the substrate upon the measurement result.[134] If such a condition cannot be met, the resulting value must be interpreted as a composite hardness. For reliable hardness and elastic (Young) modulus measurements, it is recommended to provide the load-displacement curve, which gives essential insight into the elasto-plastic properties of the indented material. Frequently, the values should be corrected for the tip geometry.[225]

In addition to indentation techniques, hardness can also be derived from microscratch measurements, in which a (usually) hemispherical diamond stylus is displaced along the sample surface with a linearly increasing load. The scratch hardness H_S is then obtained as

$$H_S = 8L/\pi l^2, \tag{6}$$

where l is the residual width of the scratch at a given load L.

The microhardness values of PECVD optical materials are summarized in Fig. 10, and they are compared with available data for PVD films and for the most frequently encountered substrates.[225] It should be pointed out here that higher H values are usually obtained for low T_S films grown at higher ion energies (typically >100 eV).

As a rule of thumb, optical materials are designated as ''hard'' when their H value is comparable or higher than that

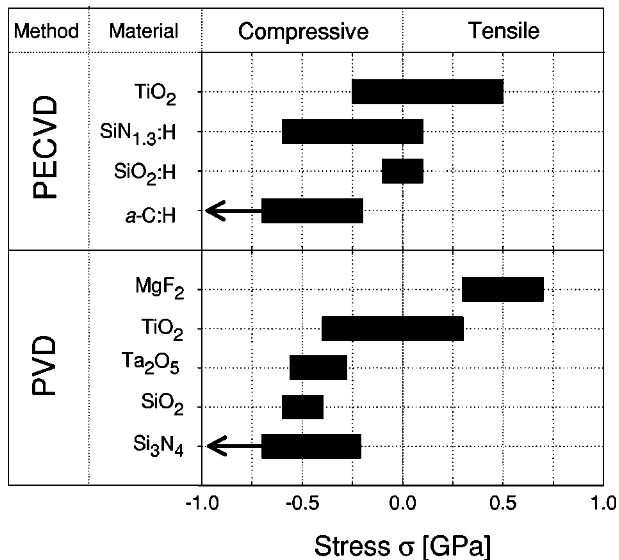

FIG. 11. Stress in different PECVD optical film materials; comparison with selected PVD materials.

of silica. This applies particularly to the films fabricated on plastic substrates. The a-C:H materials are shown here mainly for comparison: with their typical hardness of 20–40 GPa, which is about three times that of silica (a usual constituent involved in abrasive wear) they are, together with $SiN_{1.3}$:H, materials of choice for wear-resistant coatings. Very often, particularly for the case of amorphous materials, harder films generally possess a high internal stress.

Stress in thin films is closely related to the film microstructure, which is a consequence of the fabrication process: attractive forces within pores lead to tensile stress (σ_+), while gas entrapment and its physi- or chemisorption in inner cavities or at grain boundaries lead to compressive stress. In practical situations, the internal stress σ is determined from bending curvature measurements; this is expressed by the Stoney formula, developed as early as 1909[134]

$$\sigma = \frac{1}{6R}\frac{E_s d_s^2}{(1-\nu_s)d_f}, \tag{7}$$

where d is the thickness, and the subscripts s and f denote the substrate and the film, respectively. The radius R is obtained by capacitance, electromechanical, interferometric, and other measurements, usually using a circular plate or a cantilever beam.

Typical values of stress for PECVD optical materials are summarized in Fig. 11. The range of σ for each material is rather large, depending mainly on the ion bombardment energy. In fact, a transition from tensile to compressive stress has been observed for Si compound films when E_i has been increased from around 10 eV to several hundreds of eV.[226] Similarly, mostly tensile stress was reported for TiO_2 films obtained by PICVD with $E_i < 10\,\text{eV}$,[20] while compressive stress was observed for films prepared in MW/rf plasmas with E_i values of several hundreds of eV.[226] Very low $|\sigma_-|$ values were observed for hard a-C:H films ($\sigma \sim -0.2\,\text{GPa}$) obtained in MW/rf plasma.[180] A generally higher compressive stress of hydrogen-containing materials ($SiN_{1.3}$:H,a-C:H) is due to H incorporation: it has been proposed that part of the hydrogen is not chemically bonded, but it is physi- or chemisorbed on inner surfaces or trapped in the voids in the dense microstructure obtained by intense ion bombardment.[24,41,180]

Adhesion is the most important ''passive'' property of films, since it assures the integrity of the film–substrate system. Quantitatively, adhesion can be expressed by the adhesion force F_A (in Pa), i.e., a force necessary to separate two materials joined together by a common interface, or by the work of adhesion W_A (in J/m^2), which corresponds to the energy to separate two surfaces. The evaluation of adhesion may be considered from two points of view: (i) a microscopic approach, which relates adhesion to the nature of bonding at the film–substrate interface, and (ii) a macroscopic (''technological'') approach, which involves mechanical testing and stability evaluation of the film–substrate system.

Different models have been proposed to explain the phenomena responsible for adhesion; they include:[25] (i) the absorption theory, which links the bond strength to physi- and chemisorption at the interface; (ii) the electrostatic theory, associating adhesion with the action of electric charges across the film–substrate interface; (iii) the diffusion theory, linking adhesion to intermixing of the two joined materials at the interface; (iv) the rheological theory, which relates adhesion to the mechanical properties and stress distribution at the joint; and, finally (v) the mechanical interlocking theory, which explains adhesion in terms of the microgeometry at the interface.

Until now, no single theory of adhesion exists, but all of the mechanisms described above may participate in the case of optical film applications. Fabrication of optical coatings on classical substrates, such as glass, involves different cleaning steps. In the case of PECVD, the surfaces may be precleaned ''in line'' by exposure to a plasma environment (for example Ar, O_2 ...) in order to remove any weak boundary layer (WBL) arising from surface contamination (hydrocarbons, water vapor, etc.).

The situation is much more complex in the case of polymer substrates: the mechanical behavior of PECVD films on plastics, and adhesion in particular, is generally superior to that of the films fabricated by other methods, such as PVD. This fact has been related to the presence of a physically thick and structured interphase between the coating and the underlying polymer.[222] This situation is illustrated in Fig. 9 by an example for $SiN_{1.3}$:H (considered here as the first high-index material in the optical design) on PC (see Sec. III C).

Polymer surfaces are typically hydrophobic and chemically inert. Wet-chemical, flame, or corona treatments have routinely been used for adhesion improvement, but low pressure plasma modification is gaining much attention, since an appropriate control of discharge parameters may satisfy each of the above-named adhesion mechanisms. The main effects of plasma on the exposed polymer surface are:[25,26] (i) clean-

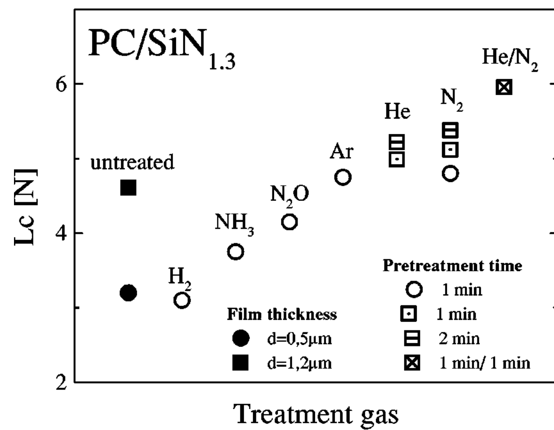

FIG. 12. Critical load L_c for $SiN_{1.3}$:H films deposited from a SiH_4/NH_3 mixture onto PC following MW plasma pretreatment in different gases (modified after Ref. 227).

ing, (ii) ablation (microetching), (iii) crosslinking, and (iv) surface-chemical functionalization.

Even if adhesion of PECVD films to polymer surfaces generally yields satisfactory results, such as passing the adhesive tape peel test, it may be further enhanced by plasma pretreatment. Adhesion improvement of $SiN_{1.3}$:H films on PC by MW plasma surface modification using different gases is illustrated in Fig. 12 in terms of critical load L_c in the microscratch analysis, where L_c is a measure of the load when the film starts to delaminate. The highest L_c values were obtained when Ar, He, and N_2 plasmas were used for pretreatment.[227] It is interesting to note that a similar result has also been observed for other combinations of materials such as SiO_2:H and $SiN_{1.3}$:H on PMMA,[228] or PP,[229] Cu on fluoropolymers,[230] or Ag on polyethylene.[231]

The above-mentioned results suggest that improved adhesion, following N_2 plasma pretreatment, is achieved due to rheological stabilization of the interphase due to crosslinking, which leads to up to a 20-fold increase of the surface microhardness.[232] This is then followed by the formation of strong, flexible, covalent linkages such as Si–N–C bonds.[222] Even if the general rules are known, plasma treatment should be optimized for each specific film–substrate combination; this is important, for example, in order to avoid cohesive failure inside the polymer,[228] or the formation of a WBL when the surface is ''overtreated,'' and low molecular weight material can be created due to polymer scission reactions.

V. EXAMPLES OF PECVD OPTICAL DEVICES

A. Optical filters

As we have seen in the previous section, PECVD can provide n_H, n_L, and n_M materials for any simple or complex optical coating systems. The designs can be based on three types of approaches: (i) multilayer (step index) design, using two or more materials, (ii) inhomogeneous (graded index) design, and (iii) quasi-inhomogeneous design, when thin ($d \ll \lambda/4$) layers with varied composition are consecutively applied, giving properties close to that of an inhomogeneous design. In this section, we give several examples of optical filters, while pointing out the necessity to precisely control the fabrication conditions.

AR coatings are traditionally the most frequently applied systems, which consist of typically 3–5 layers in the visible region.[1] In addition, they have also made their way into applications in the NIR (optoelectronics and solar cells, particularly SiN_x,[233–235] and a-C:H)[19] or deep UV (for 248 and 193 nm lithography, in order to reduce interference effects, here using TiO_2[142] and Si-rich SiN_x[233,236,237]).

When plastic substrates are used, such as in ophthalmic applications, the AR coatings are usually applied onto a hard coat. However, if deposited directly onto the polymeric substrate, special considerations should be taken into account, related to adhesion[24,51,222] and to the presence of the interphase, as already mentioned above. An example of a four layer AR system on PC is illustrated in Fig. 13.[238] An optimized W design between 450 and 650 nm, using $SiN_{1.3}$:H and SiO_2:H as n_H and n_L materials, brings the original single-side reflection of 5.0% down to about 0.8% [Fig. 13(a)]. After PECVD, a green shift of the reflectance spectrum has been observed. The means to interpret this discrepancy has been to introduce a $n(z)$ gradient, namely the presence of an interphase, in the first n_H layer[222,238] [Fig. 13(b)], a procedure which led to a good match with the experimental data [Fig. 13(c)]. Benefitting from knowledge of the existence of an interphase, a reoptimized design was then capable of further reducing the overall reflectance to ~0.7% [Fig. 13(d)].

For enhanced performance, AR coating systems are frequently provided with a water-repellent or smudge-resistant overcoat, usually employing fluorocarbon-based n_L materials, which at a small thickness ($\lesssim$10 nm), do not contribute an additional optical effect. PPFC ($n \sim 1.38$) films are being considered for such use; their surface energy is initially slightly higher than for their conventional wet- or vacuum-deposited counterparts, but they appear to exhibit a better longer-term durability.[173,177]

As mentioned earlier, PECVD is well suited for the fabrication of inhomogeneous (graded-index) coatings, such as broadband AR quintic layers or rugate filters. In this case, the n value is continuously varied between n_H and n_L, mostly by changing the gas composition,[189,131] although a variation of plasma density or of the bias potential is also possible.[131] In such approaches, at each instant of the deposition process, the $n(\lambda)$ dispersion and τ_D value must be known. A material well suited for such depositions is SiO_xN_y:H, as illustrated in Fig. 7, but Si-rich SiN_x:H/$SiN_{1.3}$:H[239] and TiO_2/SiO_2 have also been tested with success.[140]

A single-band rugate filter design with apodization leads to a reflectance spectrum with suppressed side lobes (Fig. 14). The design of rugate filters is often done by inverse Fourier-transform methods;[240–244] it is however difficult to account for $n(\lambda)$ dispersion with those techniques. In multiband rugate designs, this can be done by superposing the

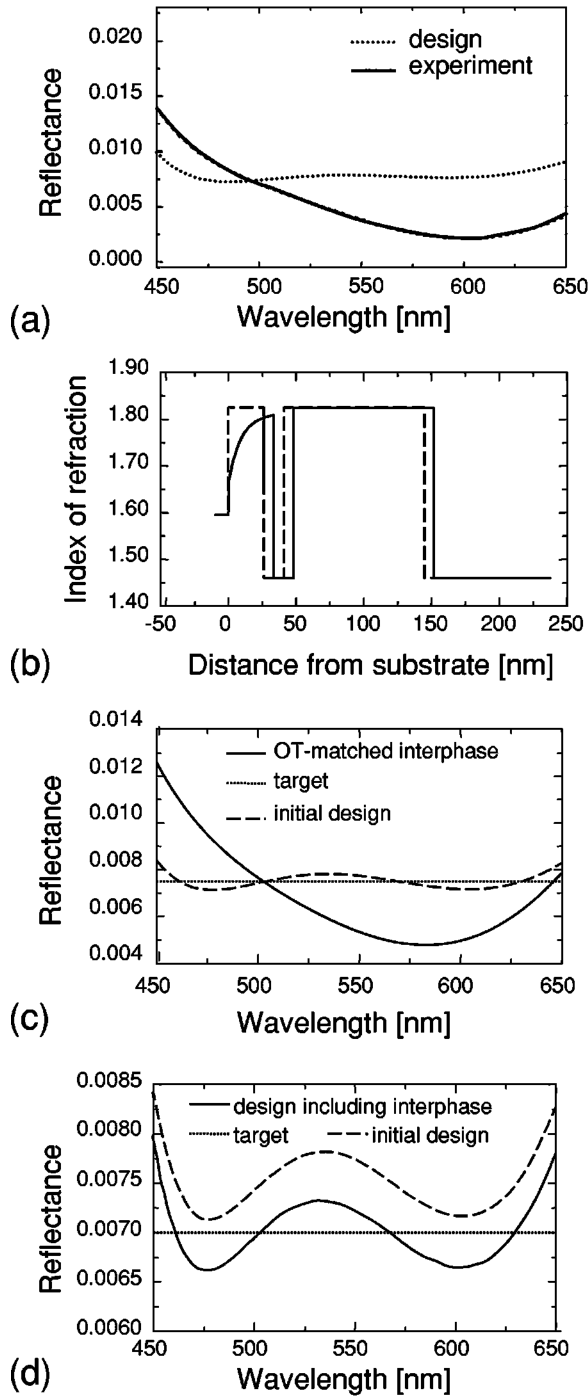

FIG. 13. Plasma-deposited AR coating on PC: (a) design; (b) experiment; (c) modified $n(z)$ profile; (d) reflectance according to (c); (d) reoptimized design (after Ref. 238).

$n_i(z)$ profiles of multiple single-band filters[242,245]

$$n(z)=n_A(z)\times n_B(z)\times n_C(z)\times \ldots, \quad (8)$$

where *A, B, C* correspond to different single-band designs, which can be calculated individually at different target wavelengths λ_A, λ_B, and λ_C, using nondispersive index values $n(\lambda_A)$, $n(\lambda_B)$, and $n(\lambda_C)$, respectively; using experimentally measured $n(\lambda)$ values, the single-band designs are redefined with respect to a common λ value, and multiplied in order to define the new multiband design. Of course, the amplitude and mean value of $n(z)$ must be corrected for the $n_{\min}$ and $n_{\max}$ available. Another way is to correct numerically the multiband design, subdividing the design into half-period sections, and optimizing the thickness and amplitude of each section to reproduce a given target. Figure 15 shows the designed $n(z)$ profile and corresponding N_2O and NH_3 measured flow-rate evolution with time, together with the measured $T(\lambda)$ spectrum of a PECVD double-band rugate filter deposited on glass [Fig. 15(d)] and PC [Fig. 15(e)].[246] It should be mentioned here that the total thickness of the example filter in Fig. 15 is about 11 μm. Complex rugate filter designs, the effect of apodization, and deposition of quasi-inhomogeneous filters, have been studied both theoretically and experimentally.[20,189] Important consequences of the inhomogeneous design are on the mechanical behavior of PECVD systems; the absence of abrupt interfaces and uniform distribution of stress lead to superior tribological properties and adhesion.[247,248]

B. Integrated optics

Research on plasma-deposited optical waveguides for integrated optics started in the early 1970s, and it has continued until now with the aim to further improve their performance (low optical loss), to increase the deposition rate, and to make them part of more sophisticated integrated optical systems. In most cases the goal has been to fabricate waveguides on silicon substrates, where the cladding layer is a thermal- or a plasma-deposited film of silicon dioxide, followed by a patterned waveguiding core layer (Fig. 16). Direct comparison of the reported optical loss values is quite difficult because of different measuring techniques and device concepts: for example, the difference Δn between n values of the core and the cladding layers determines the number of inner reflections in the waveguide and the depth of field penetration into the cladding. For smaller Δn, the effect of light scattering at the surface (or interface) roughness becomes more important while, in turn, the cladding layer may be thinner, and the evanescent wave is not attenuated by the Si substrate.

SiO_xN_y represents a good tradeoff between compactness, fiber match, fabrication complexity, and a possibility to combine optical and electronic components on one chip, compared to low-contrast technology. As the most-frequently used core-layer material, SiO_xN_y is obtained from SiH_4 mixed with N_2O or O_2. Depositions using $SiH_4/N_2O/NH_3$ or $SiH_4/N_2O/N_2$ mixtures, or with $SiN_{1.3}$ from SiH_4/NH_3 have been studied.[249–254] Although n in SiO_xN_y can vary between 1.45 and 2.00, a lower n range ($n<1.7$) is more suitable due to a smaller Δn (typically $\Delta n\sim 0.005$), and due to a lesser dependence of n on the gas flow rate ratio. As reported,[17] nonuniformity and run-to-run reproducibility of such optical waveguides is 1%–3%, while inhomogeneity and reproducibility of n is 0.7%–1.7%.

Most of the waveguiding characteristics of Si-compound films have been evaluated in the visible region, where optical loss below 0.2 dB/cm in slab waveguides and between 0.1

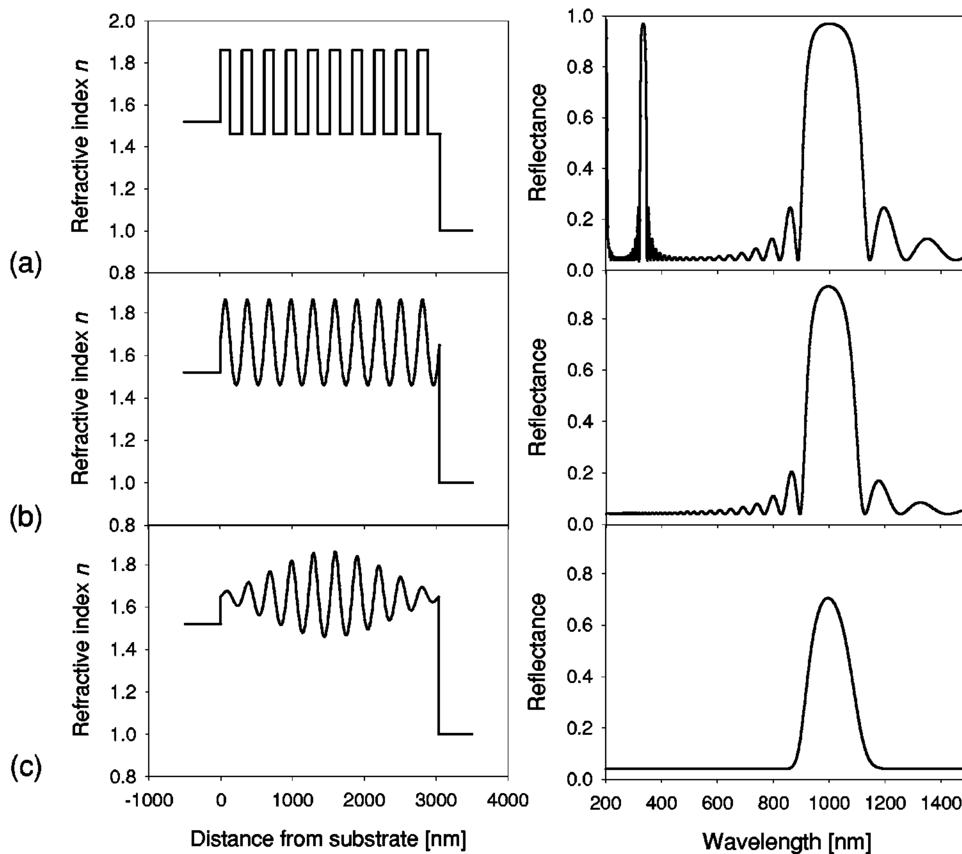

FIG. 14. Summary of filter properties: $n(z)$ profiles and $R(\lambda)$ of: (a) a multilayer, quarterwave stack; (b) a rugate filter; and (c) a rugate filter with apodization.

and 1.5 dB/cm in channel waveguides have been reported.[17,193] In the NIR region, however, the H- and N-containing films absorb due to the presence of O–H (at 1400 nm), and Si–H, thus optical losses may increase considerably (~10 dB/cm).[17] The concentrations of these groups can be reduced by postannealing: the O–H absorption has been found to disappear at 800 °C, while the N–H and Si–H contributions vanished only at 1100°, both accompanied by a substantial drop of loss. When the waveguides are fabricated on low-loss buffer layers (such as thermal SiO_2), one can change the dimensions and index of the core SiO_xN_y plasma-deposited layer and avoid the problems with IR absorption, the light propagating mostly in the cladding.[255]

Material birefringence ($\Delta n_{\text{TM-TE}}$) of SiO_xN_y has been measured ($\Delta n_{\text{TM-TE}}$ values are 0.9×10^{-3} for SiO_2, 2.3×10^{-3} when $n=1.696$, and -8.5×10^{-3} for $SiN_{1.3}$), and attributed to stress;[17] however, for $SiN_{1.3}$, it is more probably related to columnar structure, since the stress-optical coefficient values are too small to account for the measured birefringence.[256] A birefringence-compensating layer may be used in the waveguide structure, which would then contain a SiO_2 cladding, a $SiN_{1.3}$ birefringence compensating layer, and a SiO_xN_y core layer.

In addition to SiO_xN_y, other waveguiding materials and chemistries have been employed. These include SiO_2:F[257,258] or SiO_2:Ge[196,259] (losses typically 0.1–1.5 dB/cm, 0.027 dB/cm at 1.55 μm), but also organosilicones,[260–262] organometallics (Al_2O_3, ~20 dB/cm),[263] and Er-doped epitaxial Si.[264] PPFC($n=1.38$) core layers on Teflon AF cladding on Si have been considered, in view of the possibility of obtaining low optical loss in the NIR region due to the absence of O–H, Si–H, and N–H groups.[265]

Plasma-deposited Si-compound waveguides were tested on chips of integrated optical devices, such as an interferometer pressure sensor,[266] splitters,[250] and in conjunction with light emitting diodes, micromirrors and photodetectors.[267] It should be mentioned here that such device fabrication frequently combines different techniques used in various steps; besides PECVD and RIE, these can include low pressure CVD, sputtering, and implantation, among others.

As an example, a nonsymmetric Mach–Zehnder interferometer chemical sensor is shown in Fig. 16. In this configuration,[268] the light propagating along the longer branch is more affected by the surrounding medium, the refractive index of which is determined by its composition (e.g., gas or liquid solutions) than in the case of a shorter counterpart. This concept requires less fabrication steps than the symmetric interferometer sensor, which has to be equipped with a sensitizing window, but it generally provides reduced sensitivity.

Another interesting example which illustrates device fabrication is the gradient-index (GRIN) planar slab lens on Si for use in a 1×7 coupler, or for coupling between a laser diode and a waveguide[257] (Fig. 17). In this case, inhomogeneous F-doped SiO_2 (using SiH_4, O_2, and CF_4; $n=1.437-1.462$) was used with an approximately parabolic n profile, surrounded by low-index buffer layer and cladding, for a total thickness of about 24 μm. The refocusing property

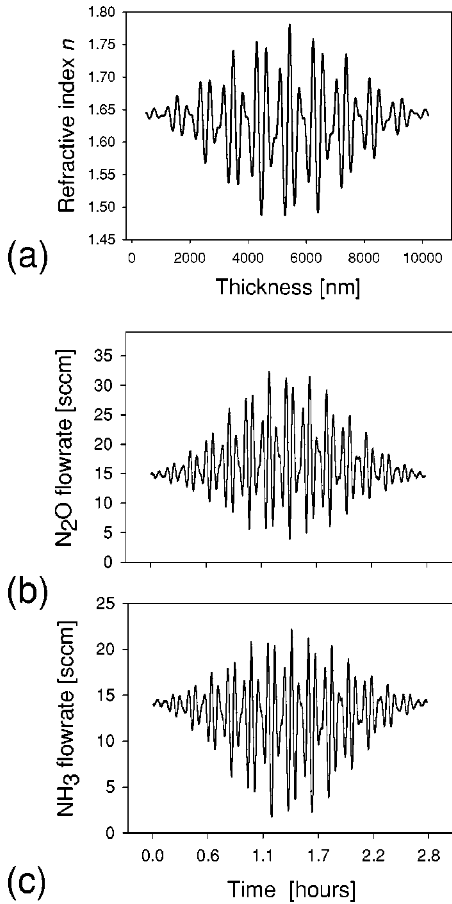

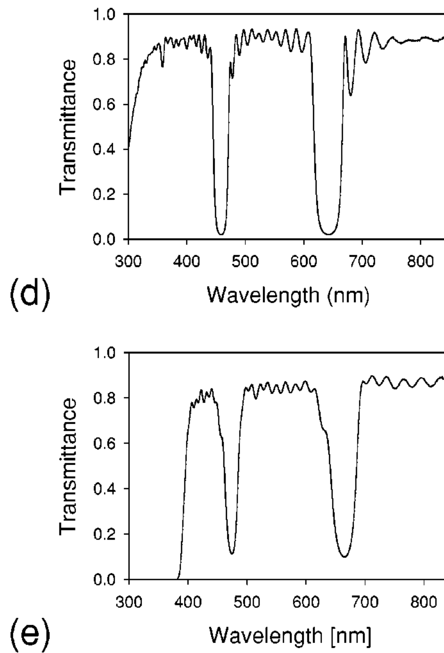

FIG. 15. Double-band rugate filters on glass: (a) design $n(z)$ profile; (b) variation with time of N_2O flow rate; (c) variation with time of NH_3 flow rate; (d) measured reflectance spectra of the resulting filter on glass; (e) similar type of coating on PC [more apodization was used in this case, suppressing sidelobes, while increasing $T(\lambda)$ in the band of interest]. Total filter thickness ~11 μm (after Ref. 246).

of the lens was demonstrated with a fluorescence microscope, using a spin-coated doped polymer on the GRIN lens. The layers were deposited at low-temperature (<250 °C), under ion bombardment (300 eV), resulting in a propagation loss of about 0.1 dB/cm. The advantage of PECVD in that case, compared to ion exchange, is that only one fabrication step is required to fabricate the GRIN.

Parallel to the integrated optics field, plasma has also been used for the deposition of Fe- or Ge-doped SiO_2 core layer on the inner surface of silica tubes for fiber optic preforms,[19,269] which actually lead to the first industrial use of PECVD for optical applications.

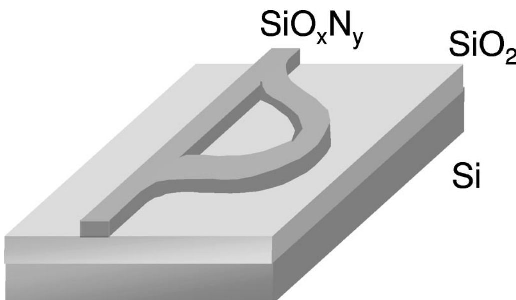

FIG. 16. Optical waveguide: nonsymmetric Mach–Zehnder interferometer sensor (after Ref. 268).

VI. PROCESS CONTROL AND INDUSTRIAL SCALE-UP

A. *In situ* monitoring and feedback control

The complexity and requirements on the control of $n(z)$ and d values in different optical film systems definitely call

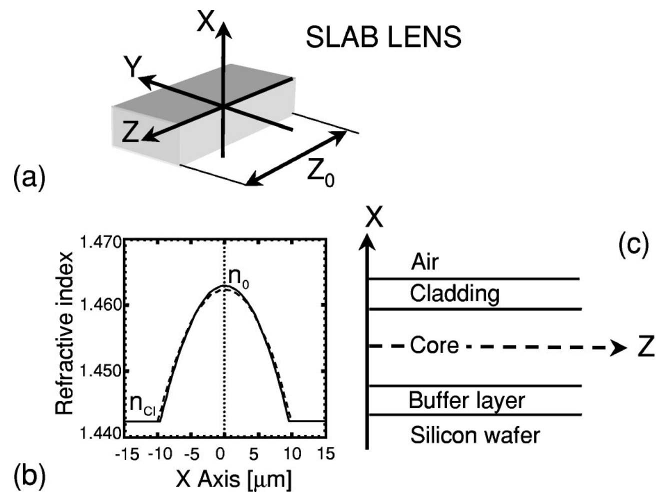

FIG. 17. Structure of PECVD GRIN slab lens showing: (a) the orientation, (b) the refractive-index profile (design and measured), and (c) the layering nomenclature (adapted from Ref. 257).

for the use of *in situ* process monitoring. The stability, reproducibility, and adjustment of the gas phase process during the PECVD can be accomplished by optical emission spectroscopy, such as in the process of growing SiO_xN_y films while monitoring the N_2^+ peak at 1009 nm,[270] in the growth of nanocomposite Au/PPFC films by monitoring the Au 287.5 nm and the CF_2 285.0 nm emission lines,[271] or by using actinometry for the control of CH radicals in the growth of SiO_2 from HMDSO/O_2 mixtures.[115] However, direct evaluation of $n(\lambda)$ and d appears to be most suitable, and this can be accomplished both by photometry and by ellipsometry, using one or multiple wavelengths (see also Sec. III A). In some cases, the light emitted from the plasma may perturb the optical monitoring; this can, however, be readily avoided by using a light source that is much more intense than the plasma glow (a laser for example), or by using a lock-in detector (expensive; single-wavelength monitoring only). When using wideband monitoring with low-intensity white sources, one must subtract the plasma emission background from the signal, assuming satisfactory plasma stability.

Ellipsometry has been shown to be the most sensitive method for monitoring optical material deposition. Recently, the use of *in situ* SE for real-time optical coating monitoring has been advanced particularly by the work of Kildemo.[272,88,191,273] Because of its phase sensitivity, ellipsometry can detect small changes of n and d: for one layer deposited, direct inversion of (Ψ, Δ) in (n, d) values has been shown to be sensitive to noise and optical singularities,[272] while better precision was obtained when fitting (n, d) for the outermost thin layer only.[274] The optical thickness is the best control variable, because it can be more precisely determined. New experimental approaches allow one to extract more information from the general Mueller matrix, which describes the polarization state of the particular system.[275]

For both reflectance and ellipsometric monitoring of coatings on transparent substrates, reflection from the back side surface of the substrate can complicate the calculation, and reflection from the substrate holder must be avoided; roughening the back surface of the substrate is a frequently used technique. In practical applications, however, back reflection is needed, so that an appropriate method must be used.[191] Real-time comparison of ellipsometric parameters with precalculated target trajectories can be used to stop the deposition of individual layers of a multilayer stack at the minimum target-measurement distance, without relying on deposition-time.[191] One can also determine the optical properties of the coating at certain critical points, and correct the ongoing design.[276] Since most substrates and films are transparent, phase-modulated ellipsometry or rotating-element ellipsometry with a compensator should be used to avoid imprecision of measurements with Δ near 0° and 180°.

Another advantage of ellipsometry is its small sensitivity to plasma emission during the measurements. So far, the method has been applied to plasma-deposited multilayers[274] and slowly varying index[88] structures. In the latter case, an elegant formulation of a generalized WKBJ approximation with first-order internal reflection was used to compute the optical properties of a slightly inhomogeneous film.[277–279] This approximation allows for fast fitting of spectra (2–3 s/fit), and for real-time monitoring of $n(z)$ in the case of transparent films. Application to coatings with more complex $n(z)$ shapes and to absorbing materials calls for the use of approximations with higher-order internal reflections. This increases the calculation time and renders such an approach still inapplicable for real-time monitoring.[88] In order to increase the speed of calculation, other optimization techniques have been investigated, such as a hybrid method using an extended Kalman filter.[280]

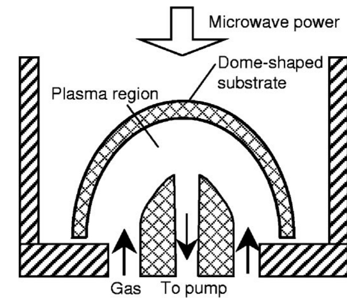

FIG. 18. Illustration of PECVD scale-up: coating of dome-shaped substrates by MW PICVD (adapted from Refs. 20 and 284).

B. Industrial scale-up

In spite of considerable efforts to develop novel optical film materials using PECVD, there are still only very few publications documenting the use of PECVD in industry. The most significant among these appears to be the PICVD process of Schott Glaswerke GmbH (see Sec. II), illustrated in Fig. 18. This approach, in which the substrate forms part of the reactor walls, was originally developed to coat the inner surface of glass tube for fiber preforms, and is now used to fabricate cold light reflectors for projection lamps and IR reflectors for energy-efficient lamps, as well as waveguides, and transparent barrier coatings.[19] The same concept can be extended to numerous other applications. Large production is achieved by increasing the total number of small deposition chambers. According to Segner,[20] annual production was 5 million lamps in 1995.

In the PICVD process, a certain film thickness (~5 nm, depending on the amount of precusors used) is deposited during each pulse of the MW power and gas injection. This approach is suitable for the fabrication of standard interference filters, but it is also appropriate to fabricate films with a quasi-inhomogeneous design (flip-flop design) based on a sequence of very thin n_H and n_L layers, giving rise to the desired n_{eff} value.

A pilot-scale, batch-continuous experimental system using the dual-mode MW/rf approach has been developed at École Polytechnique de Montréal (see Fig. 19). It allows one to accommodate a flexible substrate, 30 cm in width, for different process steps, including surface pretreatment for enhanced adhesion, alternating depositions of n_H and n_L materials, as well as of a top coat with a desired surface energy.

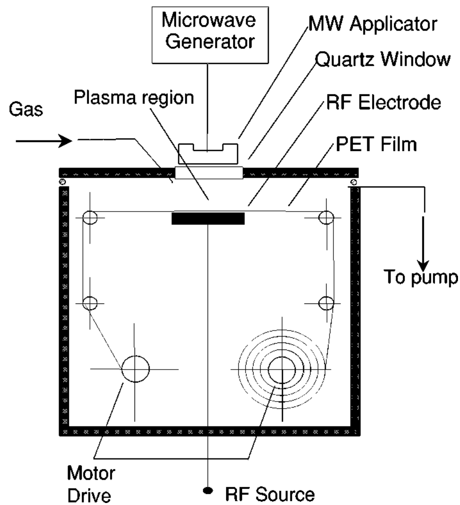

FIG. 19. MW/rf plasma system for continuous or batch deposition (from Ref. 221).

The same reactor can be applied for stationary batch coating while adopting, for example, an inhomogeneous optical design.

Other concepts of plasma systems have also been proposed for the fabrication of optical coatings, among them DECR reactors [see Fig. 3(h)].

In general, the characteristics of a suitable plasma reactor are dictated by the requirements of the desired optical system, in which the decisive factors are as follows: the choice of the n_H and n_L materials, control and reproducibility of $n(z)$, the component size and film uniformity, and the total film thickness. In addition, the deposition rate is a tradeoff between consideration of film microstructure, film stress, and precision in the thickness control. Uniformity better than 1% over 10 cm can be achieved, while a deposition rate of 1–2 nm/s is a good practical value for high quality (dense) optical coatings. It should be noted here, however, that such considerations are very general, specific aspects depending on the device to be fabricated. For example, the total thickness of AR coatings in the VIS is about 0.4 μm, while a narrowband filter in the NIR composed of several hundreds of layers may be 50 μm thick, as compared to about 10 μm thickness for a homogeneous monomode optical waveguide. Careful optimization is required to accommodate specific substrate materials (glass, polymers,...), sizes and shapes (flat, curved, rough...).

VII. CONCLUSION

The aim of the present article has been to review the advancement of knowledge on the fabrication and the characteristics of plasma-deposited optical films and coatings. We have clearly demonstrated, using available published results, that the PECVD optical films cover the same range of refractive index values as do PVD films, that is from 1.38 to 2.40 at 550 nm; this means that basically the same filter designs appropriate for PVD can also be applied in the case of PECVD. In addition, however, PECVD of optical films offers certain important advantages compared to other techniques; in particular, these are the following:

(i) PECVD makes it possible to deposit optical film systems at high rates (>1 nm/s), including the n_H material, at low T_s (ambient), over large areas, in batch or continuous modes. This is most frequently accomplished in high frequency (MW or rf) plasma systems with different levels of sophistication (independent control of E_i and ϕ_i, pulsing, etc.).

(ii) Appropriate control of the gas composition allows one to deposit multilayer interference optical systems, inhomogeneous (graded index) optical films (rugate filters), as well as films with a desired intermediate index.

(iii) PECVD is very attractive for the fabrication of optical waveguides on Si substrates; the films possess suitable optical performance ($\text{loss} < 0.2\,\text{dB/cm}$), good mechanical integrity, and they are fully compatible with the already existing Si-based fabrication technology.

(iv) Besides the desired optical characteristics, PECVD offers superior mechanical performance in terms of adhesion, stress, and hardness, and it provides additional functions such as mechanical protection (scratch-resistant hard coatings), barriers against permeation of gases or vapors, surface hydrophobicity, hydrophilicity, low friction, etc. This technique is particularly suitable for the deposition of optical films on plastic substrates, for which excellent adhesion and mechanical behavior has been demonstrated, mainly due to the presence of a physically thick interfacial region (the so-called interphase).

Even if a considerable amount of knowledge has been accumulated, there are still numerous unexplored areas, which clearly deserve attention: these include the search for novel precursors for high- and low-index materials, the fabrication of films for active devices with a simultaneous control of electrical conductivity, nonlinear optical properties, and other desirable characteristics; this can be achieved, for example, via novel nanocomposites materials, improved *in situ* control of the deposition process, different approaches facilitating the industrial scale-up, the reproducibility, etc. We trust that all these aspects will be addressed in due course, thanks to challenges being offered by optics, optical communications, and optical signal processing technology industries.

ACKNOWLEDGMENTS

The authors wish to thank Dr. Eric Kay, Dr. Jerzy A. Dobrowolski, Dr. Pat Beauchamp, Professor Michael R. Wertheimer, and Jolanta Klemberg-Sapieha, for stimulating discussions and for a critical reading of the manuscript. They also acknowledge the continuing encouragement and collaboration during the course of this work of Adam Bergeron, and Dr. Abdelbasset Hallil, Dr. Alexandru Fozza, Dr. Oleg Zabeida, Alexis Lefevre, Dan Dalacu, Dr. David Rats,

Dr. Argemiro da Silva Sobrinho, Dr. Mohamed Latrèche, and Dr. Penghui Ma. Most of this work was performed when D. Poitras was at École Polytechnique.

[1]J. A. Dobrowolski, in *Optical Society of America's Handbook of Optics*, edited by M. Bass (McGraw–Hill, New York, 1995), Chap. 42.
[2]*Thin Films for Optical Systems*, edited by F. R. Flory (Marcel Dekker, New York, 1995).
[3]R. R. Willey, Appl. Opt. **35**, 4982 (1996).
[4]*Proceedings 1st International Conference on Coatings on Glass (ICCG)*, edited by H. K. Pulker, K. Schmidt, and M. A. Aegerter (Elsevier, Amsterdam, 1997); J. Non-Cryst. Solids **218**, 1 (1997).
[5]M. Kawachi, Opt. Quantum Electron. **22**, 391 (1990).
[6]J. M. Mir and J. A. Agostinelli, J. Vac. Sci. Technol. A **12**, 1439 (1994).
[7]C. M. Lampert, working document for the International Energy Agency, task 18, advanced glazing, 1994 (unpublished).
[8]B. Hackman-Franclin, T. J. Hauser, and J. D. Jameson, U.S. Industrial Outlook 1993—Section 7, construction materials (unpublished).
[9]S. M. Reiss, Opt. Photonics News **8**, 31 (1997).
[10]J. A. Dobrowolski, K. M. Baird, P. D. Carman, and A. Wardorf, Opt. Acta **20**, 925 (1973).
[11]J. A. Dobrowolski, F. C. Ho, and A. Wardorf, Appl. Opt. **28**, 2702 (1989).
[12]R. W. Phillips and A. F. Bleikolm, Appl. Opt. **35**, 5529 (1996).
[13]R. Szipöcs, K. Ferencz, C. Spielmann, and F. Krausz, Opt. Lett. **19**, 201 (1994).
[14]F. Kartner *et al.*, Opt. Lett. **22**, 831 (1997).
[15]*Handbook of Deposition Technologies for Films and Coatings*, edited by R. F. Bunshah (Noyes, Park Ridge, NJ, 1994).
[16]*Thin Films Processes II*, edited by J. L. Vossen and W. Kern (Academic, New York, 1991).
[17]K. Wörhoff, P. V. Lambeck, and A. Driessen, J. Lightwave Technol. **17**, 1401 (1999).
[18]S. Dzioba and R. Rousina, J. Vac. Sci. Technol. B **12**, 433 (1994).
[19]*Thin Films on Glass, Schott Series on Glass and Glass Ceramics*, edited by H. Bach and D. Krause (Springer, Berlin, 1997).
[20]J. Segner, in *Thin Films for Optical Systems*, edited by F. R. Flory (Marcel Dekker, New York, 1995), Chap. 7, p. 209.
[21]Rugate (rūg·gĕt), adj. Zool. [Lat. *rūgare*] Having rugæ; wrinkled [definition found in *Oxford English Dictionary*, Oxford University Press (London, 1970)].
[22]W. H. Southwell, J. Opt. Soc. Am. A **5**, 1558 (1988).
[23]W. E. Johnson and R. L. Crane, in *Inhomogeneous and Quasi-Inhomogeneous Optical Coatings*, edited by P. G. Verly and J. A. Dobrowolski (SPIE, Bellingham, WA, 1993), Vol. 2046, pp. 88–108.
[24]L. Martinu, in *Plasma Processing of Polymers*, Applied Sciences, Vol. 346, edited by R. d'Agostino, P. Favia, and F. Fracassi (NATO ASI/Kluwer Academic, Dordrecht, 1997), pp. 247–272.
[25]E. M. Liston, L. Martinu, and M. R. Wertheimer, J. Adhes. Sci. Technol. **7**, 1091 (1993).
[26]M. R. Wertheimer and L. Martinu, in *Handbook of Thin Film Process Technology* (IOP, Bristol, 1996), Chap. E3.0.
[27]H. Biederman and L. Martinu, in *Plasma Deposition, Treatment, and Etching of Polymers*, edited by R. d'Agostino (Academic, New York, 1990), Chap. 4, pp. 269–320.
[28]C. A. Harper, *Handbook of Plastics, Elastomers and Composites* (McGraw–Hill, New York, 1992).
[29]E. Kay, J. Coburn, and A. Dilks, Top. Curr. Chem. **94**, 1 (1980).
[30]*Microwave Excited Plasmas*, edited by M. Moisan and J. Pelletier (Elsevier, Amsterdam, 1992).
[31]M. Moisan, C. Barbeau, R. Claude, C. M. Ferreira, J. Margot, J. Paraszczak, A. B. Sá, G. Sauvé, and M. R. Wertheimer, J. Vac. Sci. Technol. B **9**, 8 (1991).
[32]C. Pomot and J. Pelletier, in *Microwave Excited Plasmas*, edited by M. Moisan and J. Pelletier (Elsevier, Amsterdam, 1995), Chap. 13.
[33]R. H. Bruce, J. Appl. Phys. **52**, 7064 (1981).
[34]R. A. Roy and D. S. Yee, in *Handbook of Ion Beam Processing Technology*, edited by J. J. Cuomo, S. M. Rossnagel, and H. R. Kaufman (Noyes, Park Ridge, NJ, 1989), pp. 194–218.
[35]*Handbook of Plasma Processing Technology*, edited by S. M. Rossnagel, J. J. Cuomo, and W. D. Westwood (Noyes, Park Ridge, NJ, 1990).
[36]B. A. Movchan and A. V. Demchishin, Fiz. Met. Metalloved. **28**, 653 (1969).
[37]J. A. Thornton, J. Vac. Sci. Technol. **11**, 666 (1974).
[38]R. Messier, A. P. Giri, and R. A. Roy, J. Vac. Sci. Technol. A **2**, 500 (1984).
[39]R. Messier, J. Vac. Sci. Technol. A **4**, 490 (1986).
[40]J. M. E. Harper, J. J. Cuomo, R. J. Gambino, and H. R. Kaufman, in *Ion Bombardment Modification of Surfaces*, edited by O. Auciello and R. Kelly (Elsevier, Amsterdam, 1989), pp. 127–162.
[41]L. Martinu, J. E. Klemberg-Sapieha, O. M. Küttel, A. Raveh, and M. R. Wertheimer, J. Vac. Sci. Technol. A **12**, 1360 (1994).
[42]P. J. Kelly and R. D. Arnell, J. Vac. Sci. Technol. A **16**, 2858 (1998).
[43]J. Musil, in *Proceedings of 8th International Symposium on Elementary Processes and Chemical Reactions in Low Temperature Plasma* (Casta, Slovakia, 1992), p. 177.
[44]M. Zeuner, H. Neumann, and J. Meichsner, Vacuum **48**, 443 (1997).
[45]O. Zabeida, A. Hallil, M. R. Wertheimer, and L. Martinu, J. Appl. Phys. **88**, 635 (2000).
[46]*Plasma Deposited Thin Films*, edited by J. Mort and F. Jansen (Chemical Rubber Corp., Boca Raton, FL, 1986).
[47]Z. Zakrzewski and M. Moisan, Plasma Sources Sci. Technol. **4**, 379 (1995).
[48]J. E. Klemberg-Sapieha, O. M. Kuttel, L. Martinu, and M. R. Wertheimer, Thin Solid Films **193/194**, 965 (1990).
[49]L. Martinu, J. E. Klemberg-Sapieha, and M. R. Wertheimer, Appl. Phys. Lett. **54**, 2645 (1989).
[50]C. F. Weissfloch, M. R. Wertheimer, and R. G. Bosisio, Apparatus and Method for Plasma Generation and Material Treatment with Electromagnetic Radiation, US Patent 3814983 (1974).
[51]J. C. Rostaing, F. Coeuret, B. Drevillon, R. Etemadi, C. Godet, J. Huc, J. Y. Parey, and V. A. Yakovlev, Thin Solid Films **236**, 58 (1993).
[52]R. Etemadi, C. Godet, M. Kildemo, J. E. Bourée, R. Brenot, and B. Drévillon, J. Non-Cryst. Solids **187**, 70 (1995).
[53]R. R. Burke, J. Pelletier, C. Pomot, and L. Vallier, J. Vac. Sci. Technol. A **8**, 2931 (1991).
[54]P. Bulkin, N. Bertrand, and B. Drévillon, Thin Solid Films **296**, 66 (1997).
[55]M. Pichot, A. Durandet, J. Pelletier, Y. Armal, and L. Vallier, Rev. Sci. Instrum. **59**, 1072 (1988).
[56]M. Firon, M. C. Hugon, B. Agius, Y. Z. Hu, Y. Wang, and E. A. Irene, J. Vac. Sci. Technol. B **14**, 2543 (1996).
[57]M. Born and E. Wolf, *Principles of Optics*, 6th ed. (Pergamon, New York, 1993).
[58]F. Urbach, Phys. Rev. **89**, 1189 (1953).
[59]A. R. Forouhi and I. Bloomer, Phys. Rev. B **34**, 7018 (1986).
[60]W. A. McGahan, T. Makovicka, J. Hale, and J. A. Woollam, Thin Solid Films **253**, 57 (1994).
[61]G. E. Jellison, Jr. and F. A. Modine, Appl. Phys. Lett. **69**, 371 (1996); [Erratum: **69**, 2137 (1996)].
[62]W. E. Egan and D. E. Aspnes, Phys. Rev. B **26**, 5313 (1982).
[63]D. A. G. Bruggeman, Ann. Phys. (Leipzig) **24**, 636 (1935).
[64]D. Stroud, Phys. Rev. B **12**, 3368 (1975).
[65]A. Borghesi, E. Bellandi, G. Guizzetti, A. Sassella, S. Rojas, and L. Zanotti, Appl. Phys. A: Solids Surf. **56**, 147 (1993).
[66]S. Callard, A. Cagnaire, and J. Joseph, J. Vac. Sci. Technol. A **15**, 2088 (1997).
[67]D. E. Aspnes and J. B. Theeten, J. Appl. Phys. **50**, 4928 (1979).
[68]J. C. Garland and D. B. Tanner, eds., *Electrical Transport and Optical Properties of Inhomogeneous Media*, AIP Conf. Proc., Vol. 40 (AIP, New York, 1978).
[69]R. E. Diaz, W. M. Merrill, and N. G. Alexopoulos, J. Appl. Phys. **84**, 6815 (1998).
[70]D. E. Aspnes, in *Handbook of Optical Constants of Solids*, edited by E. D. Palik (Academic, San Diego CA, 1985), Chap. 5, pp. 89–112.
[71]D. E. Aspnes, Phys. Rev. B **41**, 10334 (1990).
[72]W. A. Pliskin, J. Vac. Sci. Technol. **14**, 1064 (1977).
[73]M. R. Wertheimer, J. E. Klemberg-Sapieha, and R. Corriveau, Can. J. Phys. **60**, 628 (1982).
[74]F. Gaillard, P. Brault, and P. Brouquet, J. Vac. Sci. Technol. A **15**, 2478 (1997).
[75]J. C. Manifacier, J. Gasiot, and J. P. Fillard, J. Phys. E **9**, 1002 (1976).
[76]R. Swanepoel, J. Phys. E **16**, 1214 (1983).
[77]J. Mouchart, G. Lagier, and B. Pointu, Appl. Opt. **24**, 1808 (1985).

[78]J. C. Martinez-Anton, in *Optical Interference Coatings*, OSA Technical Digest Series, Vol. 9 (OSA, Washington DC, 1998), p. 321.
[79]A. C. Boccara, D. Fournier, W. B. Jackson, and N. M. Amer, Opt. Lett. **5**, 377 (1980).
[80]M. Commandré and P. Roche, Appl. Opt. **35**, 5021 (1996).
[81]L. H. Sharpe, J. Adhes. **4**, 51 (1972).
[82]R. Jacobsson, in *Progress in Optics*, edited by E. Wolf (North-Holland, Amsterdam, 1966), Vol. 5, pp. 247–286.
[83]D. Tonova, A. Paneva, and B. Pantchev, Opt. Commun. **150**, 121 (1998).
[84]J. Rivory, Thin Solid Films **313–314**, 333 (1998).
[85]B. Bovard, F. J. V. Milligen, M. J. Messerly, S. G. Saxe, and H. A. Macleod, Appl. Opt. **24**, 1803 (1985).
[86]D. Poitras and L. Martinu, Appl. Opt. **37**, 4160 (1998).
[87]G. Parjadis de Larivière, J. M. Frigerio, J. Rivory, and F. Abelès, Appl. Opt. **31**, 6056 (1992).
[88]M. Kildemo, Appl. Opt. **37**, 113 (1998).
[89]R. A. B. Devine and M. Marchand, Appl. Phys. Lett. **63**, 619 (1993).
[90]Y. P. Li and W. Y. Ching, Phys. Rev. B **31**, 2172 (1985).
[91]Y.-N. Xu and W. Y. Ching, Phys. Rev. B **44**, 11048 (1991).
[92]G. Lucovsky, M. J. Manitini, J. K. Srivastava, and E. A. Irene, J. Vac. Sci. Technol. B **5**, 530 (1987).
[93]Y. Kawaguchi, Phys. Rev. B **54**, 9721 (1996).
[94]J. A. Theil, D. V. Tsu, M. W. Watkins, S. S. Kim, and G. Lucovsky, J. Vac. Sci. Technol. A **8**, 1374 (1990).
[95]S. Ogura and H. A. Macleod, Thin Solid Films **34**, 371 (1976).
[96]P. J. Martin, R. P. Netterfield, and W. G. Sainty, J. Appl. Phys. **55**, 235 (1984).
[97]N. Hirashita, S. Tokitoh, and H. Ushida, Jpn. J. Appl. Phys., Part 1 **32**, 1787 (1993).
[98]A. Gupta, S. Toby, E. P. Gusev, H. Lu, Y. Li, M. L. Green, T. Gustafsson, and E. Garfunkel, Prog. Surf. Sci. **59**, 103 (1998).
[99]A. Ricard, *Nitriding of Steel Sample by a N_2 Flowing Post-Discharge* (SFV, Paris, 1996).
[100]V. Vahedi and M. Surendra, Comput. Phys. Commun. **87**, 179 (1995).
[101]K. V. Popov, A. V. Tikhonravov, J. Campmany, E. Bertran, S. Bosch, and A. Canillas, Thin Solid Films **313–314**, 379 (1998).
[102]S. W. Hsieh, C. Y. Chang, and S. C. Hsu, J. Appl. Phys. **74**, 2638 (1993).
[103]S. M. Han and E. S. Aydil, J. Vac. Sci. Technol. A **14**, 2062 (1996).
[104]N. Bertrand, B. Drévillon, and P. Bulkin, J. Vac. Sci. Technol. A **16**, 63 (1998).
[105]K. Ishii, Y. Ohki, and H. Nishikawa, J. Appl. Phys. **76**, 5418 (1994).
[106]K. H. A. Bogart, S. K. Ramirez, L. A. Gonzales, G. R. Bogart, and E. R. Fisher, J. Vac. Sci. Technol. A **16**, 3175 (1998).
[107]G. M. Jellum and D. B. Graves, Appl. Phys. **67**, 1716 (1990).
[108]M. Shiratani, S. Matsuo, and Y. Watanabe, Jpn. J. Appl. Phys., Part 1 **30**, 1887 (1991).
[109]Y. Watanabe and M. Shiratani, Jpn. J. Appl. Phys., Part 1 **32**, 3074 (1993).
[110]A. Love, S. Middleman, and A. K. Hochberg, J. Cryst. Growth **129**, 119 (1993).
[111]S. C. Deshmukh and E. S. Aydil, J. Vac. Sci. Technol. A **13**, 2355 (1995).
[112]R. P. Mota, D. Galvão, S. F. Durrant, M. A. B. de Moraes, S. de Oliveira Dantas, and M. Cantão, Thin Solid Films **270**, 109 (1995).
[113]A. Goullet, F. Nicolazo, G. Turban, A. Granier, and C. Vallée, J. Non-Cryst. Solids **216**, 77 (1997).
[114]L. Zajíčková, I. Ohlídal, and J. Janča, Thin Solid Films **280**, 26 (1996).
[115]R. Lamendola, P. Favia, F. Palumbo, and R. d'Agostino, Eur. Phys. J.: Appl. Phys. **4**, 65 (1998).
[116]B. G. Bovard, in *Thin Films for Optical Systems*, edited by F. R. Flory (Marcel Dekker, New York, 1995), Chap. 5, pp. 117–132.
[117]W. G. Sainty, W. D. McFall, D. R. McKenzie, and Y. Yin, Appl. Opt. **34**, 5659 (1995).
[118]C. Vallée, A. Goullet, F. Nicolazo, A. Granier, and G. Turban, J. Non-Cryst. Solids **311**, 212 (1997).
[119]S. Garcia, J. M. Martin, I. Martil, M. Fernandez, E. Iborra, and G. Gonzalez-Diaz, J. Non-Cryst. Solids **187**, 329 (1995).
[120]D. L. Smith, J. Vac. Sci. Technol. A **111**, 1843 (1993).
[121]J. Robertson, Philos. Mag. B **63**, 47 (1991).
[122]Z. Yin and F. W. Smith, Phys. Rev. B **42**, 3658 (1990).
[123]Z. Yin and F. W. Smith, Phys. Rev. B **42**, 3666 (1990).
[124]D. E. Kotecki and J. D. Chapple-Sokol, J. Appl. Phys. **77**, 1284 (1995).
[125]B. F. Hanyaloglu and E. S. Aydil, J. Vac. Sci. Technol. A **16**, 2794 (1998).
[126]J. Petalas and S. Logothetidis, Phys. Rev. B **50**, 11801 (1994).
[127]D. V. Tsu, G. Lucovsky, and M. J. Mantini, Phys. Rev. B **33**, 7069 (1986).
[128]A. Hofrichter, P. Bulkin, and B. Drévillon, Appl. Surf. Sci. **142**, 447 (1999).
[129]F. L. Martínez, I. Mártil, G. González-Díaz, B. Selle, and I. Sieber, J. Non-Cryst. Solids **227–230**, 523 (1998).
[130]O. Sanchez, M. A. Aguilar, C. Falcony, J. M. Martinez-Duart, and J. M. Albella, J. Vac. Sci. Technol. A **14**, 2088 (1996).
[131]D. Poitras, P. Leroux, J. E. Klemberg-Sapieha, S. C. Gujrathi, and L. Martinu, Opt. Eng. **35**, 2693 (1996).
[132]T. P. Smirnova and L. V. Yakovkina, Thin Solid Films **293**, 6 (1997).
[133]F. Fracassi, R. d'Agostino, and G. Bruno, Plasmas Polymers **1**, 3 (1996).
[134]M. Ohring, *The Materials Science of Thin Films* (Academic, Boston, MA, 1992).
[135]P. J. Martin, A. Bendavid, and H. Takikawa, J. Vac. Sci. Technol. A **17**, 2351 (1999).
[136]Y. H. Lee, K. K. Chan, and M. J. Brady, J. Vac. Sci. Technol. A **13**, 596 (1995).
[137]H. Schroeder, in *Oxide Layers Deposited from Organic Solutions*, edited by G. Hass and R. E. Thun (Academic, New York, 1969), Vol. 5, pp. 87–141.
[138]L. M. Williams and D. W. Hess, J. Vac. Sci. Technol. A **1**, 1810 (1983).
[139]L. M. Williams and D. W. Hess, Thin Solid Films **115**, 13 (1984).
[140]L. Martinu, M. Latrèche, V. Hajek, J. E. Klemberg-Sapieha, A. Argoitia, and P. Beauchamp, *Proceedings of the 43rd Annual Technical Conference* (Society of Vacuum Coaters, Denver, 2000), p. 177.
[141]H. J. Frenck, W. Kulisch, M. Kuhr, and R. Kassing, Thin Solid Films **201**, 327 (1991).
[142]B.-H. Jun *et al.*, Appl. Opt. **36**, 1482 (1997).
[143]H.-K. Ha, M. Yoshimoto, H. Koinuma, B.-K. Moon, and H. Ishiwara, Appl. Phys. Lett. **68**, 2965 (1996).
[144]W. G. Lee, S. I. Woo, J. C. Kim, S. H. Choi, and K. H. Oh, Thin Solid Films **237**, 105 (1994).
[145]J.-W. Kim, D.-O. Kim, and Y.-B. Hahn, Korean J. Chem. Eng. **15**, 217 (1998).
[146]I.-S. Lee, J.-W. Kim, C.-J. Youn, S.-K. Park, and Y.-B. Hahn, Korean J. Chem. Eng. **13**, 473 (1996).
[147]Y. H. Lee, Vacuum **51**, 503 (1998).
[148]H. Sankur and W. Gunning, J. Appl. Phys. **66**, 4747 (1989).
[149]J. Nair, P. Nair, F. Mizukami, Y. Oosawa, and T. Okubo, Mater. Res. Bull. **34**, 1275 (1999).
[150]J.-S. Chen, S. Chao, J.-S. Kao, G.-R. Lai, and W.-H. Wang, Appl. Opt. **36**, 4403 (1997).
[151]K. Bange, Fresenius J. Anal. Chem. **353**, 240 (1995).
[152]T. Goto, W. Zhang, and T. Hirai, Jpn. J. Appl. Phys., Part 1 **38**, 3668 (1999).
[153]J. Patscheiber and S. Veprek, Plasma Chem. Plasma Process. **12**, 129 (1992).
[154]C. E. Chryssou and C. W. Pitt, Appl. Phys. A: Mater. Sci. Process. **65**, 469 (1997).
[155]C. E. Chryssou and C. W. Pitt, IEEE J. Quantum Electron. **34**, 282 (1998).
[156]R. A. B. Devine, L. Vallier, J. L. Autran, P. Paillet, and J. L. Leray, Appl. Phys. Lett. **68**, 1775 (1996).
[157]M. T. Weise, S. C. Selbrede, L. J. Arias, and D. Carl, J. Vac. Sci. Technol. A **15**, 1399 (1997).
[158]K. Ishii, A. Takami, and Y. Ohki, J. Appl. Phys. **81**, 1470 (1997).
[159]H. Kudo, R. Shinohara, S. Takeishi, N. Awaji, and M. Yamada, Jpn. J. Appl. Phys., Part 1 **35**, 1583 (1996).
[160]W.-T. Tseng, Y.-T. Hsieh, C.-F. Lin, M.-S. Tsai, and M.-S. Feng, J. Electrochem. Soc. **144**, 1100 (1997).
[161]V. L. Shannon and M. Z. Karim, Thin Solid Films **270**, 498 (1995).
[162]M. Yoshimaru, S. Koizumi, and K. Shimokawa, J. Vac. Sci. Technol. A **15**, 2908 (1997).
[163]S. Hasegawa, T. Tsukaoka, T. Inokuma, and Y. Kurata, J. Non-Cryst. Solids **240**, 154 (1998).
[164]J. H. Lee, D. S. Kim, and Y. H. Lee, J. Electrochem. Soc. **143**, 1443 (1996).
[165]D. R. Denison, J. C. Barbour, and J. H. Burkhard, J. Vac. Sci. Technol. A **14**, 1124 (1996).
[166]S. W. Lim, Y. Shimogaki, Y. Nakano, K. Tada, and H. Komiyama, Jpn. J. Appl. Phys., Part 1 **35**, 1468 (1996).

[167]H. Kitoh, M. Muroyama, M. Sasaki, M. Iwasawa, and H. Kimura, Jpn. J. Appl. Phys., Part 1 **35**, 1464 (1996).
[168]S.-M. Yun, H.-Y. Chang, K.-M. Lee, D.-C. Kim, and C.-K. Choi, J. Electrochem. Soc. **145**, 2576 (1998).
[169]S. M. Han and E. S. Aydil, J. Appl. Phys. **83**, 2172 (1998).
[170]J. H. Lowry, J. S. Mendlowitz, and N. S. Subramanian, Opt. Eng. **31**, 1982 (1992).
[171]D. M. Manos and D. L. Flamm, *Plasma Etching: An Introduction* (Academic, Boston, MA, 1989).
[172]C. B. Labelle and K. K. Gleason, J. Vac. Sci. Technol. A **17**, 445 (1999).
[173]O. Takai, A. Hozumi, and N. Sugimoto, J. Non-Cryst. Solids **218**, 280 (1997).
[174]A. Weber, R. Pöchelmann, and C.-P. Klages, J. Vac. Sci. Technol. A **16**, 2120 (1998).
[175]U. Hetzler and E. Kay, J. Appl. Phys. **49**, 5617 (1978).
[176]L. Martinu, H. Biederman, and J. Nedbal, Thin Solid Films **136**, 11 (1986).
[177]J. E. Klemberg-Sapieha, L. Martinu, V. Fridman, and D. E. Morton, in *Proceedings of the 41st Annual Technical Conferences* (Society of Vacuum Coaters, Albuquerque, NM, 1998), p. 138.
[178]J. Robertson, in *Diamond and Diamond-Like Films and Coatings, NATO-ASI Series B: Physics*, NATO ASI, edited by R. Clausing, L. Horton, J. Angus, and P. Koidl (Plenum, New York, 1991), pp. 331–356.
[179]*Properties and Characterization of Amorphous Carbon Films, Materials Science Forum*, Vols. 52–53, edited by J. Pouch and S. A. Alterovitz (Trans.-Tech., Aedermannsdorf, Switzerland, 1990).
[180]L. Martinu, A. Raveh, D. Boutard, S. Houle, D. Poitras, N. Vella, and M. R. Wertheimer, Diamond Relat. Mater. **2**, 673 (1993).
[181]D. Das Gupta, F. Demichelis, C. F. Pirri, R. Spagnolo, and A. Tagliaferro, in *Diamond and Diamond-Like Films and Coatings*, edited by R. E. Clausing (Plenum, New York, 1991), pp. 427–437.
[182]H. Sjötröm, S. Stafström, M. Boman, and J.-E. Sundgren, Phys. Rev. Lett. **75**, 1336 (1995).
[183]N. Hellgren, M. P. Johansson, E. Broitman, L. Hultman, and J.-E. Sundgren, Phys. Rev. B **59**, 5162 (1999).
[184]B. Kleinorge, A. C. Ferrari, J. Robertson, W. I. Milne, S. Waidmann, and S. Hearne, Diamond Relat. Mater. **9**, 643 (2000).
[185]R. E. Sah, B. Dischler, A. Bubenzer, and P. Koidl, Appl. Phys. Lett. **46**, 739 (1985).
[186]*Diamond: Electronic Properties and Applications*, edited by L. S. Pan and D. R. Kania (Kluwer Academic, Dordrecht, 1995).
[187]*Applications of Diamond Films and Related Materials*, NIST Special Publication, Vol. 885, edited by A. Feldman, Y. Tzeng, W. A. Yarbrough, M. Yoshikawa, and M. Murakawa (National Institute of Standards and Technology, Washington DC, 1995).
[188]C. F. M. Borges, M. Moisan, and A. Gicquel, Diamond Relat. Mater. **4**, 149 (1995).
[189]A. C. Greenham, B. A. Nichols, R. M. Wood, N. Nourshargh, and K. L. Lewis, Opt. Eng. **32**, 1018 (1993).
[190]P. V. Bulkin, P. L. Swart, and B. M. Lacquet, J. Non-Cryst. Solids **187**, 484 (1995).
[191]M. Kildemo, P. Bulkin, B. Drévillon, and O. Hunderi, Appl. Opt. **36**, 6352 (1997).
[192]S. Lim, J. H. Ryu, J. F. Wager, and T. K. Plant, Thin Solid Films **245**, 141 (1994).
[193]L. Martinu, in *Functional Photonic and Fiber Devices*, edited by S. I. Najafi and M. N. Armenise (SPIE, Bellingham, WA, 1994), Vol. 2695, pp. 30–37.
[194]C. M. M. Denisse, K. Z. Troost, J. B. O. Elferink, F. H. P. M. Habraken, and M. Hendriks, J. Appl. Phys. **60**, 2536 (1986).
[195]H. G. Tompkins, R. B. Gregory, P. W. Deal, and S. M. Smith, J. Vac. Sci. Technol. A **17**, 391 (1999).
[196]T. Hattori, S. Semura, and N. Akasaka, Jpn. J. Appl. Phys., Part 1 **38**, 2775 (1999).
[197]G. F. Zhang, L. J. Guo, Z. T. Liu, X. K. Xiu, and X. Zhong, Appl. Opt. **76**, 705 (1994).
[198]S. F. Durrant, S. G. Castro, J. I. Cisneros, N. C. d. Cruz, and M. A. B. de Moraes, J. Vac. Sci. Technol. A **14**, 118 (1996).
[199]U. Kreibig and P. Zacharias, Z. Phys. **231**, 128 (1970).
[200]D. Ricard, P. Roussignol, and C. Flytzanis, Opt. Lett. **10**, 511 (1985).
[201]F. Hache, D. Ricard, C. Flytzanis, and U. Kreibig, Appl. Phys. A: Solids Surf. **47**, 347 (1988).
[202]H. B. Liao, R. R. Xiao, J. S. Fu, P. Yu, G. K. L. Wong, and P. Sheng, Appl. Phys. B: Lasers Opt. **65**, 673 (1997).
[203]H. B. Liao, R. F. Xiao, J. S. Fu, H. Wang, K. S. Wong, and G. K. L. Wong, Opt. Lett. **23**, 388 (1998).
[204]B. Abeles, Appl. Solid State Sci. **6**, 1 (1976).
[205]D. Dalacu and L. Martinu, J. Vac. Sci. Technol. A **17**, 877 (1999).
[206]S. Veprˇek, J. Vac. Sci. Technol. A **17**, 2401 (1999).
[207]F. Arefi-Khonsari, F. Hellegouarc'h, and J. Amouroux, J. Vac. Sci. Technol. A **16**, 2240 (1998).
[208]F. Arefi-Khonsari, F. Hellegouarc'h, R. Planade, and J. Amouroux, Mater. Res. Soc. Symp. Proc. **544**, 129 (1999).
[209]E. Márquez, P. Nagels, J. M. González-Leal, A. M. Bernal-Oliva, E. Sleeckx, and R. Callaerts, Vacuum **52**, 55 (1999).
[210]J. W. Yi, Y. H. Lee, and B. Farouk, Thin Solid Films **326**, 154 (1998).
[211]K. Itoh and O. Matsumoto, Thin Solid Films **345**, 29 (1999).
[212]M. R. Wertheimer, A. C. Fozza, and A. Holländer, Nucl. Instrum. Methods Phys. Res. B **151**, 65 (1999).
[213]L. Escoubas, A. Gatto, G. Albrand, P. Roche, and M. Commandré, Appl. Opt. **37**, 1883 (1998).
[214]*The Properties of Optical Glass, Schott Series on Glass and Glass Ceramics*, edited by H. Bach and N. Neuroth (Springer, Berlin, 1995).
[215]J. A. Kerr, in *CRC Handbook of Chemistry and Physics*, edited by D. R. Lide (Chemical Rubber Corp., Boca Raton, FL, 1999), pp. 9–51.
[216]A. Rivaton and J. Gardette, Angew. Makromol. Chem. **261/262**, 173 (1998).
[217]A. Bergeron, J. E. Klemberg-Sapieha, and L. Martinu, J. Vac. Sci. Technol. A **16**, 3227 (1998).
[218]A. C. Fozza, J. Roch, J. E. Klemberg-Sapieha, A. Kruse, A. Holländer, and M. R. Wertheimer, Nucl. Instrum. Methods Phys. Res. B **131**, 205 (1997).
[219]*Plastics Additives Handbook*, 4th ed., edited by R. Gächter, H. Müller, and P. P. Klemchuk (Hanser, Munich, 1993).
[220]A. Holländer, J. E. Klemberg-Sapieha, and M. R. Wertheimer, J. Polym. Sci., Part A: Polym. Chem. **34**, 1511 (1996).
[221]A. S. da Silva Sobrinho, N. Schüler, J. E. Klemberg-Sapieha, M. R. Wertheimer, M. Andrews, and S. C. Gujrathi, J. Vac. Sci. Technol. A **16**, 2021 (1998).
[222]J. E. Klemberg-Sapieha, D. Poitras, L. Martinu, N. L. S. Yamasaki, and C. W. Lantman, J. Vac. Sci. Technol. A **15**, 985 (1997).
[223]A. Bergeron, D. Poitras, and L. Martinu, Opt. Eng. **39**, 825 (2000).
[224]B. Bhushan, *Handbook of Micro/Nano Tribology* (Chemical Rubber Corp., Boca Raton, FL, 1995).
[225]W. C. Oliver and J. M. Pharr, J. Mater. Res. **7**, 1564 (1992).
[226]J. E. Klemberg-Sapieha, L. Martinu, M. R. Wertheimer, P. Gunther, R. Schellin, C. Thielemann, and G. Sessler, J. Vac. Sci. Technol. A **14**, 2775 (1996).
[227]J. E. Klemberg-Sapieha, S. Dahl, and L. Martinu, *Proceedings 43rd Annual Technical Conference* (Society of Vacuum Coaters, Denver, 2000), p. 234.
[228]J. E. Klemberg-Sapieha, L. Martinu, N. L. S. Yamasaki, and C. W. Lantman, Mater. Res. Soc. Symp. Proc. **544**, 277 (1998).
[229]S. Vallon, B. Drévillon, F. Poncin-Epaillard, J. E. Klemberg-Sapieha, and L. Martinu, J. Vac. Sci. Technol. A **14**, 3194 (1996).
[230]M. K. Shi, A. Selmani, L. Martinu, E. Sacher, M. R. Wertheimer, and A. Yelon, J. Adhes. Sci. Technol. **8**, 1129 (1994).
[231]L. J. Gerenser, J. Vac. Sci. Technol. A **6**, 2897 (1988).
[232]S. Dahl, D. Rats, J. von Stebut, L. Martinu, and J. E. Klemberg-Sapieha, Thin Solid Films **355–356**, 290 (1999).
[233]P. Doshi, G. E. Jellison, Jr., and A. Rohatgi, Appl. Opt. **36**, 7826 (1997).
[234]S. Winderbaum, F. Yun, and O. Reinhold, J. Vac. Sci. Technol. A **15**, 1020 (1997).
[235]L. Asinovsky, F. Shen, and T. Yamaguchi, Thin Solid Films **313–314**, 198 (1998).
[236]Z.-T. Jiang, T. Yamaguchi, K. Ohshimo, M. Aoyama, and L. Asinovsky, Jpn. J. Appl. Phys., Part 1 **37**, 571 (1998).
[237]F. Gaillard, P. Schiavone, and P. Brault, J. Vac. Sci. Technol. A **15**, 2777 (1997).
[238]D. Poitras and L. Martinu, Appl. Opt. **39**, 1168 (2000).
[239]P. L. Swart, P. V. Bulkin, and B. M. Lacquet, Opt. Eng. **36**, 1215 (1997).
[240]E. Delano, J. Opt. Soc. Am. **57**, 1529 (1967).
[241]L. Sossi, Izv. Akad. Nauk Estonskoi SSR, Fizika, Matematika **23**, 229 (1974).
[242]J. A. Dobrowolski and D. Lowe, Appl. Opt. **17**, 3039 (1978).

[243]P. G. Verly and J. A. Dobrowolski, Appl. Opt. **29**, 3672 (1990).
[244]A. V. Tikhonravov, B. T. Sullivan, and M. V. Borisova, Appl. Opt. **33**, 5142 (1994).
[245]B. G. Bovard, Appl. Opt. **32**, 5427 (1993).
[246]D. Poitras, Ph.D. thesis, École Polytechnique de Montréal, January 2000.
[247]D. Rats, D. Poitras, J. M. Soro, L. Martinu, and J. von Stebut, Surf. Coat. Technol. **111**, 220 (1999).
[248]D. Rats, J. M. Soro, L. Martinu, and J. von Stebut, Surf. Coat. Technol. **123**, 36 (2000).
[249]S. Sriram, W. D. Partlow, and C. S. Liu, Appl. Opt. **22**, 3664 (1983).
[250]D. K. W. Lam, Appl. Opt. **23**, 2744 (1984).
[251]D. E. Bossi, J. M. Hammer, and J. M. Shaw, Appl. Opt. **26**, 609 (1987).
[252]K. Kapser, C. Wagner, and P. P. Deimel, IEEE Trans. Photonics Technol. Lett. **3**, 1096 (1991).
[253]F. Bruno, M. del Guidice, R. Recca, and F. Testa, Appl. Opt. **30**, 4560 (1991).
[254]G. Giroult-Matlakowski, C. Charles, A. Durandet, R. W. Boswell, S. Armand, H. M. Persing, A. J. Perri, P. D. Lloyd, and S. C. Hyde, J. Vac. Sci. Technol. A **12**, 2754 (1994).
[255]M. Hoffmann, P. Kopka, and E. Voges, IEEE Photonics Technol. Lett. **9**, 1238 (1997).
[256]A. Durandet and D. R. McKenzie, J. Appl. Phys. **80**, 4707 (1996).
[257]D. R. Beltrami, J. D. Love, A. Durandet, A. Samoć, and C. J. Cogswell, Appl. Opt. **36**, 7143 (1997).
[258]M. V. Bazylenko, M. Gross, A. Simonian, and P. L. Chu, J. Vac. Sci. Technol. A **14**, 336 (1996).
[259]N. Nourshargh, E. M. Starr, and J. S. McCormack, IEE Proc. J: Optoelectron. **133**, 264 (1986).
[260]P. K. Tien, G. Smolinsky, and R. J. Martin, Appl. Opt. **11**, 637 (1972).
[261]M. Tabasky, E. S. Bulat, B. Tweed, and C. Herrick, J. Vac. Sci. Technol. A **12**, 1244 (1994).
[262]E. S. Bulat, M. Tabasky, B. Tweed, C. Herrick, S. Hankin, N. J. Lewis, D. Oblas, and T. Fitzgerald, J. Vac. Sci. Technol. A **11**, 1268 (1993).
[263]A. H. Bailey, D. A. Darbyshire, A. P. Overbury, and C. W. Pitt, Vacuum **36**, 139 (1986).
[264]J. L. Rogers, W. J. Varhue, E. Adams, M. A. Lavoie, and R. O. Frenette, J. Vac. Sci. Technol. A **12**, 2762 (1994).
[265]W. Wirges, S. Bauer-Gogonea, S. Bauer, R. Gerhard-Multhaupt, L. Martinu, J. E. Klemberg-Sapieha, and M. R. Wertheimer, Proc. SPIE **2213**, 303 (1994).
[266]C. Wagner, J. Frankenberger, and P. P. Deimel, IEEE Photonics Technol. Lett. **5**, 1257 (1993).
[267]S. Yokoyama *et al.*, J. Vac. Sci. Technol. A **13**, 629 (1995).
[268]A. Malek-Tabrizi, S. I. Najafi, and L. Martinu, in *Functional Photonic and Fiber Devices*, edited by S. I. Najafi and M. N. Armenise (SPIE, Bellingham WA, 1996), Vol. 2695, p. 180.
[269]*Fiber Optics and Glass Integrated Optics*, Schott Series on Glass and Glass Ceramics, edited by H. Bach and D. Krause (Springer, Berlin, to be published).
[270]L. Pinard and J. M. Mackowski, Appl. Opt. **36**, 5451 (1997).
[271]L. Martinu and H. Biederman, Plasma Chem. Plasma Process. **5**, 81 (1985).
[272]M. Kildemo and B. Drévillon, Rev. Sci. Instrum. **67**, 1956 (1996).
[273]M. Kildemo, B. Drévillon, and O. Hunderi, Thin Solid Films **313–314**, 484 (1998).
[274]M. Kildemo, S. Deniau, P. Bulkin, and B. Drévillon, Thin Solid Films **290–291**, 46 (1996).
[275]S. Y. Kim, Appl. Opt. **35**, 6703 (1996).
[276]B. T. Sullivan and J. A. Dobrowolski, Appl. Opt. **31**, 3821 (1995).
[277]M. Kildemo, O. Hunderi, and B. Drévillon, J. Opt. Soc. Am. A **14**, 931 (1997).
[278]L. M. Brekhovskikh, *Waves in Layered Media* (Academic, New York, 1980), p. 199.
[279]J. R. Wait, *Electromagnetic Waves in Stratified Media* (Pergamon, New York, 1962), p. 88.
[280]C. G. Galarza, P. P. Khargonekar, N. Layardi, T. L. Vincent, E. A. Rietman, and J. T. C. Lee, Thin Solid Films **313–314**, 156 (1998).
[281]*Handbook of Optical Constants of Solids*, edited by E. D. Palik (Academic, San Diego, CA, 1991).
[282]VASE Software, version 3.142, J. A. Woollam Co.
[283]D. Dalacu and L. Martinu, J. Appl. Phys. **87**, 228 (2000).
[284]Schott Glasswork, H. W. Erbsom, H. Krümmel, H. Pacquet, and G. Weidmann, Eur. Pat. EP-446596A.